ARL 70-0139

A THEORY OF TWO-DIMENSIONAL AIRFOILS WITH STRONG INLET FLOW ON THE UPPER SURFACE

SEDAT SERDENGECTI
FRANK E. MARBLE

CALIFORNIA INSTITUTE OF TECHNOLOGY
PASADENA, CALIFORNIA

AUGUST 1970

CONTRACT NO. F33615-68-C-1013
PROJECT NO. 7064

AEROSPACE RESEARCH LABORATORIES
AIR FORCE SYSTEMS COMMAND
UNITED STATES AIR FORCE
WRIGHT-PATTERSON AIR FORCE BASE, OHIO

FOREWORD

This final report on Contract F33615-68-C-1013 covers work carried out at The California Institute of Technology from 1 November 1967 to 31 December 1969. This research was supported in part under the ARL In-House Independent Laboratory Research Funds. The Project Engineer monitoring this contract was Dr. K. S. Nagaraja, Hypersonic Research Laboratory, ARL. Technical contributions to the work were made by Dr. S. Serdengecti, Dr. W. D. Rannie, Dr. F. E. C. Culick, Dr. E. E. Zukoski and the Principal Investigator, Dr. Frank E. Marble.

ABSTRACT

The two-dimensional theory of airfoils with arbitrarily strong inlet flow into the upper surface was examined with the aim of developing a thin-airfoil theory which is valid for this condition. Such a theory has, in fact, been developed and reduces uniformly to the conventional thin-wing theory when the inlet flow vanishes. The integrals associated with the arbitrary shape, corresponding to the familiar Munk integrals, are somewhat more complex but not so as to make calculations difficult.

To examine the limit for very high ratios of inlet to free-stream velocity, the theory of the Joukowski airfoil was extended to incorporate an arbitrary inlet on the upper surface. Because this calculation is exact, phenomena observed in the limit cannot be attributed to the linearized calculation.

These results showed that airfoil theory, in the conventional sense, breaks down at very large ratios of inlet to free-stream velocity. This occurs where the strong induced field of the inlet dominates the free-stream flow so overwhelmingly that the flow no longer leaves the trailing edge but flows toward it. Then the trailing edge becomes, in fact a leading edge and the Kutta condition is physically inapplicable. For the example in this work, this breakdown occurred at a ratio of inlet to free-stream velocity of about 10. This phenomena suggests that for ratios in excess of the critical value, the flow separates from the trailing edge and the circulation is dominated by conditions at the edges of the inlet.

TABLE OF CONTENTS

LIST OF ILLUSTRATIONS

1. INTRODUCTION

Fan-in-wing or submerged engine installations present novel aerodynamic problems associated with interaction of the inlet and discharge flow fields with lifting surfaces, control surfaces, and fuselage. This interaction is most important during flight modes for which the inlet velocity is much larger than the forward speed of the aircraft.[1] When the inlet flow does not separate it closely resembles a potential field and consequently the induced loads on lifting surfaces may be very important. As a consequence, the inlet flow merits investigation quite apart from the exhaust flow field.

Flow fields induced by inlets on the upper surfaces of wings lie outside the framework of thin airfoil theory because those calculations are based upon linearization with the undisturbed free stream velocity. Within this theory, velocities normal to the undisturbed flow, such as an inlet flow, must be small in comparison with the free stream velocity. Actually, the opposite is more frequently true.

The aim of the present analysis has been to develop the rudiments of a two-dimensional airfoil theory capable of treating arbitrary ratios of upper-surface inlet velocity to free stream velocity and still retain the essential simplicity and flexibility of conventional linearized airfoil theory. This is done with the full recognition that in practice the flow field exhibits stronger three-dimensionality than conventional wings. As usual, however, the two-dimensional theory demonstrates in a simple

manner a lift and moment characteristic similar to the three-dimensional one that may be extracted only with some difficulty from three-dimensional numerical calculations. It is equally true that two-dimensional results for strong upper-surface inlet flow must be used with even more caution than their conventional counterparts.

In the present work, a general analysis is developed for thin wings with arbitrarily strong inlet on the upper surface. To accomplish this, the linearization is carried out with respect to the exact potential field of a flat plate with the desired inlet flow embedded in it. In order to examine the flow field apart from the thin wing limitations, the familiar Joukowski airfoil theory is extended to include an arbitrary inlet flow in the upper surface.

2. FLAT PLATE WITH DISTRIBUTED SUCTION

The uniform rectilinear flow over flat plate at angle of attack α, having a strong distributed suction over a portion of the upper surface, constitutes the basic flow for the perturbation theory of thin airfoils. Characteristically, it also provides some of the most interesting results in their most elementary form.

Consider a flow in the z $(\equiv x+iy)$ plane in which all lengths have been made dimensionless through division by $c/4$; c is the physical chord of the airfoil after mapping. In a corresponding manner, velocities are made dimensionless through division by U_0 , the free

stream velocity. Then the complex potential for the circle $|z| = 1$ is

$$W_1(z) = z e^{-i\alpha} + 1/z e^{-i\alpha} - \frac{i\Gamma}{2\pi U_0 c/4} \log z \qquad (2.1)$$

where Γ is the as yet undetermined circulation required to establish the stagnation point at $z = 1$. On this circle, figure 1, we wish to establish an inlet flow with velocity $V_0(\psi)$ normal to this circle with ψ, the angle referring to location of an inlet element, lying in the range $\psi_1 \leq \psi \leq \psi_2$. An element of inlet flow may be established by situating a sink at the point in question together with the regular potential required to satisfy the condition that the remainder of the circle remains a streamline. This flow may be obtained directly from the well-known potential for a source of strength m located at a point z_1 exterior to the circle.[2] This complex potential is

$$\frac{m}{2\pi} \log \left\{ \frac{(z - z_1)(z - 1/\bar{z}_1)}{z} \right\}$$

Now if we permit the location z_1 of the singularity to approach the desired location $e^{i\psi}$ of our inlet element and interpret $m = -V_0(\psi)(c/4)\,d\psi$ as the inlet volume flow over the element of circumferential extent $d\psi$, then the potential to be superposed upon the existing field (2.1) is

$$\frac{-V_0(\psi)\,d\psi}{2\pi U_0} \log \left\{ (z - e^{i\psi})^2 / z \right\} \qquad (2.2)$$

where the dimensionless complex potential has been used. The complete potential in the circle plane is therefore

$$W(z) = z e^{-i\alpha} + 1/z e^{i\alpha} - \frac{i\Gamma}{2\pi U_0 c/4} \log z - \frac{1}{2\pi} \int_{\psi_1}^{\psi_2} \frac{V_0(\psi)}{U_0} \log \left\{ (z - e^{i\psi})^2 / z \right\} d\psi \tag{2.3}$$

The circulation Γ required to set the stagnation point at $z = 1$ is determined by the condition that $\frac{dW}{dz}(1) = 0$. This gives

$$-\frac{i\Gamma}{2\pi U_0 c/4} = 2i \sin\alpha + \frac{1}{2\pi} \int_{\psi_1}^{\psi_2} \frac{V_0(\psi)}{U_0} \left(\frac{1 + e^{i\psi}}{1 - e^{i\psi}} \right) d\psi \tag{2.4}$$

where the second term on the left hand side is the contribution to the circulation resulting from the inlet flow.

In the plane of the flat plate, the lengths and velocities are likewise made dimensionless through division by $c/4$ and U_0 respectively. Then the transformation to the ζ $(\equiv \xi + i\eta)$ plane takes the form

$$\zeta = z + 1/z \tag{2.5}$$

so that the circle $|z| = 1$ maps into the slit along the ξ axis in the region $-2 \leq \xi \leq 2$. In physical dimensions, the leading and trailing edges are situated at $-c/2$ and $c/2$ respectively and the physical chord is c.

The force and moment characteristics of the flat plate are both

fundamental and interesting. They may be found by utilizing the dimensionless complex conjugate velocity

$$\frac{dW(z)}{dz} = e^{-i\alpha} - e^{i\alpha}\cdot\frac{1}{z^2} + 2i\sin\alpha\cdot\frac{1}{z}$$

$$-\frac{1}{\pi}\int_{\psi_1}^{\psi_2}\left\{\frac{1}{z-e^{i\psi}} - \frac{1}{1-e^{i\psi}\cdot\frac{1}{z}}\right\}\frac{V_0(\psi)}{U_0}\,d\psi \qquad (2.6)$$

in Blasius first integral

$$\frac{F_\xi - iF_\eta}{\frac{1}{2}\rho U_0^2 c} = \frac{i}{4}\oint\left(\frac{dW(\zeta)}{d\zeta}\right)^2 d\zeta = \frac{i}{4}\oint\left(\frac{dW(z)}{dz}\right)^2\frac{dz}{d\zeta}\,dz \qquad (2.7)$$

The last integral is carried out in the z plane and

$$\frac{dz}{d\zeta} = \frac{z^2}{z^2-1} \qquad (2.8)$$

follows from the transformation function. The forces F_ξ and F_η are the actual dimensional forces acting on the flat plate. By considering the contour for large values of z the residue in (2.7) is easily calculated and the forces are

$$\frac{F_\xi - iF_\eta}{\frac{1}{2}\rho U_0^2 c} = \frac{i}{4}\cdot 2\pi i\cdot 2e^{-i\alpha}\left\{2i\sin\alpha + \frac{1}{\pi}\int_{\psi_1}^{\psi_2}\frac{e^{i\psi}}{1-e^{i\psi}}\cdot\frac{V_0(\psi)}{U_0}\,d\psi\right\}$$

Simplifying and taking the complex conjugate,

$$\frac{F_\xi + i F_\eta}{\frac{1}{2}\rho U_0^2 c} = e^{i(\alpha + \pi/2)} \left\{ 2\pi \sin\alpha + \frac{1}{2}\int_{\psi_1}^{\psi_2} \operatorname{ctn}\left(\frac{\psi}{2}\right) \cdot \frac{V_0}{U_0}\, d\psi - \frac{i}{2}\int_{\psi_1}^{\psi_2} \frac{V_0}{U_0}\, d\psi \right\} \tag{2.9}$$

The component normal to the flow direction is designated lift while that parallel to the flow direction is the drag. Thus, the lift and drag coefficients are respectively

$$C_L = 2\pi \sin\alpha + \frac{1}{2}\int_{\psi_1}^{\psi_2} \operatorname{ctn}\left(\frac{\psi}{2}\right) \cdot \frac{V_0(\psi)}{U_0}\, d\psi \tag{2.10}$$

and

$$C_D = \frac{1}{2}\int_{\psi_1}^{\psi_2} \frac{V_0(\psi)}{U_0}\, d\psi \tag{2.11}$$

The drag coefficient represents simply the "sink drag" associated with the inlet flow.[3] The integral in equation (2.10) is due to the additional circulation about the plate caused by the suction. The suction clearly induces an up-flow about the trailing edge which requires an additional circulation to satisfy the Kutta condition.

The counterclockwise moment about the midpoint of the airfoil follows from Blasius second integral, taking account of the dimensionless representations we have used

$$\frac{M}{U_0^2 (c/4)^2} = -\frac{1}{2}\rho \, Re \oint \left(\frac{dW(\zeta)}{d\zeta}\right)^2 \zeta \, d\zeta$$

Utilizing the mapping relation so that the integral may be evaluated in the circle plane; the moment coefficient becomes

$$C_M \equiv \frac{M}{\frac{1}{2}\rho U_0^2 c^2} = -\frac{1}{16} Re \oint \left(\frac{dW(z)}{dz}\right)^2 \left(\frac{z^2+1}{z^2-1}\right) z \, dz \qquad (2.12)$$

From the expression for the conjugate velocity given in equation (2.6), the integral is most easily evaluated by considering the contour at large $|z|$ values. After a modest calculation the moment coefficient may be written explicitly,

$$4 C_M = -2\pi \cos\alpha \cdot \sin\alpha - 2\int_{\psi_1}^{\psi_2} \sin\tfrac{1}{2}\psi \cdot \cos\left(\tfrac{1}{2}\psi - \alpha\right) \cdot \frac{V_0}{U_0} \, d\psi$$

$$- \frac{1}{4\pi}\left[\int_{\psi_1}^{\psi_2} \cot\tfrac{1}{2}\psi \cdot \frac{V_0}{U_0} \, d\psi\right]\int_{\psi_1}^{\psi_2} \frac{V_0}{U_0} \, d\psi \qquad (2.13)$$

The first term on the right hand side represents the familiar moment coefficient associated with the flat plate at angle of attack α. The remaining two terms are associated with the intake. The first of these integrals results from the intake impulse and its orientation with respect to the angle of attack. The last term, although independent of the angle of attack, is geometrically associated with the flat plate since it arises

from satisfying the Kutta condition at the trailing edge. Note that if the problem had been treated as if the inlet velocity, as well as the angle of attack, was small, the last term in (2.13) would not be present and the second term would be independent of angle of attack. That is, for small α and $|V_0/U_0|$

$$4C_M = -2\pi \sin\alpha - \int_{\psi_1}^{\psi_2} \sin\psi \cdot \frac{V_0}{U_0}\, d\psi \tag{2.14}$$

On the other hand, when V_0/U_0 is permitted to be large, as is true in the cases of physical interest, the assumption of small angle of attack leads to

$$4C_M = -\left[2\pi + \int_{\psi_1}^{\psi_2} (1-\cos\psi)\frac{V_0}{U_0}\, d\psi\right] \sin\alpha - \int_{\psi_1}^{\psi_2} \sin\psi \cdot \frac{V_0}{U_0}\, d\psi$$

$$- \frac{1}{4\pi}\left[\int_{\psi_1}^{\psi_2} \operatorname{ctn}\tfrac{1}{2}\psi \cdot \frac{V_0}{U_0}\, d\psi\right]\int_{\psi_1}^{\psi_2} \frac{V_0}{U_0}\, d\psi \tag{2.15}$$

Clearly, this difference becomes quite important for large V_0/U_0 and therefore justifies the treatment carried out here.

For the specific example where the inlet velocity in the circle plane is constant and extends from $\psi_1 = \pi/4$ to $\psi_2 = 3\pi/4$, the airfoil characteristics may be written, when the angle of attack is small,

$$C_L = 2\pi \sin\alpha + \frac{V_0}{U_0} \log\left(\operatorname{ctn}\frac{\pi}{8}\right) \tag{2.16}$$

$$C_D = \frac{\pi}{4} \cdot \frac{V_0}{U_0} \tag{2.17}$$

$$4C_M = -2\pi\left(1 + \frac{1}{4}\frac{V_0}{U_0}\right)\sin\alpha - \sqrt{2}\,\frac{V_0}{U_0}$$

$$-\frac{1}{4}\left(\frac{V_0}{U_0}\right)^2 \log\left(\operatorname{ctn}\frac{\pi}{8}\right) \tag{2.18}$$

For values of $\frac{V_0}{U_0} > 10$, the moment coefficient is dominated by the term which would be absent in conventional linearized theory.

3. THIN AIRFOIL WITH STRONG DISTRIBUTED SUCTION

The results of the previous section emphasize the importance of large ratios of suction to free-stream velocity and show that the linearization which assumes V_0/U_0 small cannot safely be extended to large values. As a consequence, conventional thin-airfoil theory cannot be extended to this case; the entire thin-wing theory must be extended and reworked.

The conventional thin-wing theory utilizes, in a sense, the potential motion about a flat plate, or a circle, as the basic field about which the perturbation is carried out. The perturbation consists in modifying the shape slightly to achieve camber and thickness or, what is the same, modifying the shape of the circle slightly before mapping.

It is appropriate, therefore, to consider the flat plate with suction as the exact potential field about which perturbations are carried out.

Then the complete range of values for $|V_0/U_0|$ is retained while small cambers and thicknesses may be achieved.

In the dimensionless circle plane, figure 2, let $\beta(\vartheta)$ be the radial increment of the thin airfoil map with respect to the circle.[4] The polar coordinates of this map are $1+\beta(\vartheta)$, ϑ so that $|\beta(\vartheta)| << 1$ when the airfoil is thin. Our perturbation analysis requires that we (a) find the regular complex perturbation potential $w^{(1)}(z)$ such that (b) the complete potential describes a flow tangential to the perturbed contour. In keeping with our first-order perturbation analysis we must find the radial velocity to be prescribed on the unit circle which satisfies this boundary condition. Referring to figure 2, the flow will follow the prescribed contour if

$$\int_0^{\vartheta} V_r(1,\vartheta')\,d\vartheta' = \int_1^{1+\beta(\vartheta)} V_\theta(r',\theta)\,dr' \tag{3.1}$$

where primes denote variables of integration. This relation holds for all values of ϑ and thus, with the linear perturbation theory, the radial velocity required on the unit circle is

$$V_r^{(1)}(1,\vartheta) = \frac{d}{d\theta}\left\{\beta(\theta)\,V_\theta^{(0)}(1,\theta)\right\} \tag{3.2}$$

where $V_\theta^{(0)}(1,\theta)$ is the tangential velocity of the unperturbed flow at the unit circle. $V_r^{(1)}(1,\vartheta)$ is a perturbation quantity, as a consequence of equation (3.2) and the definition of $\beta(\vartheta)$.

The difference between the present problem and conventional thin-wing theory is apparent in equation (3.2). For conventional thin-wing theory $V_\theta^{(0)}(1,\vartheta)$ is the tangential velocity for uniform flow about the unit circle; for the present analysis $V_\theta^{(0)}(1,\theta)$ includes also the velocity induced on the circle by the inlet flow.

The complex perturbation potential $W^{(1)}(z)$, which must be added to (2.3), (2.4) to achieve the desired solution, has three obvious restrictions.

1) $W^{(1)}(z)$ must be regular outside the unit circle;

2) $W^{(1)}(z)$ must have no net source strength within the unit circle;

3) the uniform flow must be unaltered at large distances from the circle.

This potential is then of the form

$$W^{(1)}(z) = \frac{-i\,\Gamma^{(1)}}{2\pi V_0\, c/4} \log z + \sum_1^\infty C_n z^{-n} \tag{3.3}$$

where the $\Gamma^{(1)}$ is the additional circulation required to establish the Kutta condition in the perturbed flow field and the $C_n = A_n + iB_n$ are complex constants. The real part of $W^{(1)}$, the perturbation velocity potential, is

$$\varphi^{(1)}(r,\theta) = \frac{\Gamma^{(1)}}{2\pi V_0\, c/4}\cdot\vartheta + \sum_1^\infty \left\{ \frac{A_n}{r^n}\cos n\vartheta + \frac{B_n}{r^n}\sin n\vartheta \right\} \tag{3.4}$$

and the radial velocity perturbation on the unit circle may be written

$$\frac{V_r^{(1)}(1,\vartheta)}{U_0} = -\sum_1^\infty n A_n \cos n\vartheta - \sum_1^\infty n B_n \sin n\vartheta \tag{3.5}$$

Now since $V_r^{(1)}(1,\vartheta)$ is known from equation (3.2) for the boundary condition, the Fourier coefficients are

$$A_n = -\frac{1}{n\pi}\int_0^{2\pi} \frac{V_r^{(1)}}{U_0}(1,\vartheta)\cos n\vartheta \, d\vartheta$$

$$B_n = -\frac{1}{n\pi}\int_0^{2\pi} \frac{V_r^{(1)}}{U_0}(1,\vartheta)\sin n\vartheta \, d\vartheta \tag{3.6}$$

The value of $\Gamma^{(1)}$ follows from the Kutta condition,

to be

$$\frac{\Gamma^{(1)}}{2\pi U_0 c/4} = -\sum_1^\infty n B_n \tag{3.7}$$

Formally, then, the C_n and $\Gamma^{(1)}$ are known in terms of the given airfoil shape so that the perturbation potential $W^{(1)}(z)$ is completely determined.

Knowledge of the airfoil contour implies that the coordinate η of the contour is given in terms of chordwise distance ξ measured from the midpoint of the chordline. But the transformation relation (2.5) gives,

for small deviations from the circle

$$\xi = 2\cos\vartheta$$

and consequently,

$$\eta(\xi) = 2\beta(\vartheta)\sin\vartheta$$

and hence the airfoil shape is related to the circle distortion $\beta(\theta)$ as

$$\beta(\theta) = \frac{1}{2}\,\frac{\eta(2\cos\vartheta)}{\sin\vartheta} \tag{3.8}$$

The radial perturbation velocity at the circle, required in the determination of the Fourier coefficients, is then

$$\frac{V_r^{(1)}}{U_0} = \frac{1}{2}\,\frac{d}{d\vartheta}\left\{\frac{V_\vartheta^{(0)}}{U_0}\cdot\frac{\eta(2\cos\vartheta)}{\sin\vartheta}\right\} \tag{3.9}$$

The tangential velocity $V_\vartheta^{(0)}$ on the unperturbed circle with suction follows from equation (2.6) which, with some rearrangement, gives

$$\frac{V_\vartheta^{(0)}}{U_0} = -2\sin\vartheta + \frac{1}{2\pi}\int_{\psi_1}^{\psi_2}\left\{\operatorname{ctn}\left(\frac{\psi-\vartheta}{2}\right) - \operatorname{ctn}\left(\frac{\psi}{2}\right)\right\}\frac{V_\infty}{U_0}\,d\psi \tag{3.10}$$

where the angle of attack α has been treated as a perturbation term. The Fourier coefficients may then be written explicitly

$$\begin{Bmatrix} A_n \\ B_n \end{Bmatrix} = \frac{1}{n\pi} \int_0^{2\pi} \frac{d}{d\theta} \left\{ \eta(2\cos\theta) \right\} \begin{Bmatrix} \cos n\theta \\ \sin n\theta \end{Bmatrix} d\theta$$

$$- \frac{1}{4\pi} \int_{\psi_1}^{\psi_2} \frac{V_0}{U_0} d\psi \cdot \frac{1}{n\pi} \int_0^{2\pi} \frac{d}{d\theta} \left\{ \left[\operatorname{ctn}\left(\frac{\psi-\theta}{2}\right) - \operatorname{ctn}\left(\frac{\psi}{2}\right) \right] \left[\frac{\eta(2\cos\theta)}{\sin\theta} \right] \right\} \begin{Bmatrix} \cos n\theta \\ \sin n\theta \end{Bmatrix} d\theta \qquad (3.11)$$

The complex potential for the thin airfoil with prescribed shape is then given as the sum of equations (2.3) [with (2.4)] and equation (3.3), with coefficients determined using equations (3.7) and (3.11).

4. LIFT, DRAG, AND MOMENT OF THIN WING WITH STRONG SUCTION

The force and moment coefficients for the arbitrary thin airfoil may now be computed utilizing the Blasius integrals and the complex perturbation potential developed in the previous section. We take the complex velocity in the form

$$u - iv = e^{-i\alpha} - e^{i\alpha} \frac{1}{z^2} - \frac{1}{\pi} \int_{\psi_1}^{\psi_2} \left\{ \frac{1}{z - e^{i\psi}} - \left(\frac{1}{1 - e^{i\psi}} \right) \frac{1}{z} \right\} \frac{V_0}{U_0} d\psi$$

$$+ (2i\sin\alpha) \frac{1}{z} + i \sum_1^\infty n B_n \cdot \frac{1}{z^n} - \sum_1^\infty n C_n \frac{1}{z^{n+1}} \qquad (4.1)$$

The evaluation of contour integrals for forces and moments involves consideration of the integrand for large values of the variable in the z plane. Consequently, it is appropriate to rearrange equation (4.1) in descending powers of z . This requires only the expansion of the first term in the integral. The appropriate expression for $u - iv$ is then

$$u - iv = e^{-i\alpha} + \left\{ \frac{1}{2\pi} \int_{\psi_1}^{\psi_2} \frac{i e^{i\psi/2}}{\sin \psi/2} \frac{V_0}{U_0} d\psi + 2i \sin\alpha + i \sum_1^\infty n B_n \right\} \frac{1}{z}$$

$$- \left\{ e^{i\alpha} + C_1 + \frac{1}{\pi} \int_{\psi_1}^{\psi_2} e^{i\psi} \frac{V_0}{U_0} d\psi \right\} \frac{1}{z^2}$$

$$- \sum_2^\infty \left[n C_n + \frac{1}{\pi} \int_{\psi_1}^{\psi_2} e^{in\psi} \frac{V_0}{U_0} d\psi \right] \frac{1}{z^{n+1}} \tag{4.2}$$

Now since

$$\frac{z^2}{z^2 - 1} = \sum_0^\infty z^{-2n} \tag{4.3}$$

the force integral, which contains the integrand

$$(u - iv)^2 \cdot \frac{z^2}{z^2 - 1} \tag{4.4}$$

has the residue

$$e^{-i\alpha} \left\{ 2i \sin\alpha + i \sum_1^\infty n B_n + \frac{i}{2\pi} \int_{\psi_1}^{\psi_2} \frac{e^{i\psi/2}}{\sin \psi/2} \frac{V_0}{U_0} d\psi \right\} \tag{4.5}$$

If we complete evaluation of the contour integral and take the complex conjugate of the force, the force in the airfoil plane is

$$\frac{F_\xi + i F_\eta}{U_0^2\, c/4} = 2\pi\rho e^{i\alpha}\left\{ 2i\sin\alpha + i\sum_1^\infty n B_n + \frac{1}{2\pi}\int_{\psi_1}^{\psi_2} \frac{V_0}{U_0}\, d\psi \right.$$

$$\left. + \frac{i}{2\pi}\int_{\psi_1}^{\psi_2} \operatorname{ctn}\psi/2 \cdot \frac{V_0}{U_0}\, d\psi \right\} \tag{4.5}$$

The force coefficient is obtained in convenient form by a slight rearrangement to give

$$\frac{F_\xi + i F_\eta}{\frac{1}{2}\rho U_0^2 c} = e^{i(\alpha + \pi/2)}\left\{ 2\pi\sin\alpha + \pi\sum_1^\infty n B_n + \frac{1}{2}\int_{\psi_1}^{\psi_2} \operatorname{ctn}\psi/2 \cdot \frac{V_0}{U_0}\, d\psi \right.$$

$$\left. - \frac{1}{2} i \int_{\psi_1}^{\psi_2} \frac{V_0}{U_0}\, d\psi \right\} \tag{4.6}$$

The components parallel to and normal to the free stream are now clear so that we can write down lift and drag coefficients immediately

$$C_L = 2\pi\left(\sin\alpha + \frac{1}{2}\sum_1^\infty n B_n\right) + \frac{1}{2}\int_{\psi_1}^{\psi_2} \operatorname{ctn}\psi/2\, \frac{V_0}{U_0}\, d\psi \tag{4.7}$$

$$C_D = \frac{1}{2}\int_{\psi_1}^{\psi_2} \frac{V_0}{U_0}\, d\psi \tag{4.8}$$

Comparison with the flat-plate results, equations (2.10) and (2.11), reveals that the only modification is the effect of additional circulation resulting from profile shape, $\pi \sum_1^\infty n B_n$. This result is exactly the one we would have obtained by simply adding the flat-plate inlet effect to the conventional thin-airfoil solution. Thus, there is no coupling between the strong inlet flow and the airfoil shape in the force coefficients.

As noted in Section 2, the moment involves an integrand

$$(u-iv)^2 \frac{z^2+1}{z^2-1} z \tag{4.9}$$

where

$$\frac{z^2+1}{z^2-1} z = z\left(1+\frac{1}{z^2}\right) \cdot \sum_0^\infty z^{-2n} \tag{4.10}$$

The residue is determined then by a straightforward multiplication of the power series for large z , utilizing the expression for $u-iv$ given by equation (4.1). The result for the residue is

$$-2e^{-i\alpha}\left[e^{i\alpha} + C_1 + \frac{1}{\pi}\int_{\psi_1}^{\psi_2} e^{i\psi}\frac{V_e}{U_0}\,d\psi\right] + 2\left[e^{-i\alpha}\right]^2$$

$$+\left[2i\sin\alpha + i\sum_1^\infty n B_n + \frac{i}{2\pi}\int_{\psi_1}^{\psi_2}\frac{e^{i\psi/2}}{\sin\psi/2}\frac{V_e}{U_0}\,d\psi\right]^2 \tag{4.11}$$

Thus, the dimensionless moment in the airfoil plane, measured in a counterclockwise sense, is $\pi\rho\, q_\infty \{\text{residue}\}$ where the residue is

that given by equation (4. 11). The result of this calculation is

$$\frac{M}{U_0^2(c/4)^2} = \pi\rho\left\{-4\cos\alpha\sin\alpha - \frac{2}{\pi}\int_{\psi_1}^{\psi_2}\sin(\psi-\alpha)\cdot\frac{V_0}{U_0}\,d\psi + 2A_1\sin\alpha\right.$$

$$\left. - 2B_1\cos\alpha - \left[2\sin\alpha + \sum_1^\infty nB_n + \frac{1}{2\pi}\int_{\psi_1}^{\psi_2}\cot\psi/2\cdot\frac{V_0}{U_0}\,d\psi\right]\frac{1}{\pi}\int_{\psi_1}^{\psi_2}\frac{V_0}{U_0}\,d\psi\right. \tag{4. 12}$$

If we now recall that, in keeping with small perturbation theory, A_n, B_n, and α are small, some obvious terms of the second and higher order may be dropped, so that the moment coefficient becomes

$$4C_M = -\left[2\pi + \int_{\psi_1}^{\psi_2}(1-\cos\psi)\frac{V_0}{U_0}\,d\psi\right]\sin\alpha - \int_{\psi_1}^{\psi_2}\sin\psi\,\frac{V_0}{U_0}\,d\psi$$

$$-\pi B_1 - \left[\frac{1}{2}\sum_1^\infty nB_n + \frac{1}{4\pi}\int_{\psi_1}^{\psi_2}\cot\frac{\psi}{2}\cdot\frac{V_0}{U_0}\,d\psi\right]\int_{\psi_1}^{\psi_2}\frac{V_0}{U_0}\,d\psi \tag{4. 13}$$

The treatment for large inlet velocities contributes two terms that would not be recovered within the usual linearized airfoil theory. The first,

$$-\int_{\psi_1}^{\psi_2}(1-\cos\psi)\,\frac{V_0}{U_0}\,d\psi\cdot\sin\alpha \tag{4. 14}$$

arises from the circulation increase with angle of attack associated with the intake velocity. This term is independent of the airfoil shape and,

indeed, it is present in the flat plate result given in equation (2.15). The second term in question is

$$-\frac{1}{2}\sum_{1}^{\infty} n B_n \int_{\psi_1}^{\psi_2} \frac{V_0}{U_0}\, d\psi \qquad (4.15)$$

which represents the coupling between inlet flow and the circulation induced by the airfoil shape. Both of these terms assume significant proportions for V_0/U_0 large, as occurs in near-hovering flight.

5. AN ELEMENTARY EXAMPLE

Consider an airfoil with upper surface intake which extends from $\psi_1 = \pi/4$ to $\psi_2 = 3\pi/4$ in the circle plane and for which the intake velocity V_0 is uniform. The intake is then symmetrically located on the airfoil. For purposes of illustration, the shape will be taken as

$$\begin{aligned} \eta &= 0 && \text{on the upper surface,} \\ \eta &= -\tau \sin\vartheta && \text{on the lower surface.} \end{aligned} \qquad (5.1)$$

Because of the nature of the dimensionless quantities used, the dimensionless "thickness" τ is the ratio of the actual thickness to $c/4$, the characteristic length. The thickness of our example, which is provided entirely by the lower surface contour, is actually $(c/4)\tau$.

In the airfoil plane, the shape may be written conveniently by recalling that the horizontal coordinate ξ is related to the angle ϑ in the circle plane as $\xi/2 = \cos\vartheta$. Hence, the airfoil shape is

$$\begin{aligned} \eta &= 0 && \text{upper surface} \\ \eta &= -\tau\sqrt{1-(\xi/2)^2} && \text{lower surface} \end{aligned} \tag{5.2}$$

This contour, together with the location of the upper surface intake, is shown in figure 3. Clearly, the shape is given by

$$\left(\frac{\xi}{2}\right)^2 + \left(\frac{\eta}{\tau}\right)^2 = 1 \tag{5.3}$$

so that the lower surface is elliptical, with a semi-major axis of 2 and a semi-minor axis of τ .

To compute values for the lift, drag, and moment coefficients, we are required to find values of the coefficients B_n . Referring to equation (3.11), we must evaluate

$$B_n = \frac{1}{n\pi}\int_{\pi}^{2\pi} \frac{d}{d\vartheta}\left\{-\tau\sin\vartheta\right\}\sin n\vartheta\, d\vartheta$$

$$+ \frac{1}{4\pi}\int_{\pi/4}^{3\pi/4} \frac{V_0}{U_0}\, d\psi \cdot \frac{\tau}{n\pi}\int_{\pi}^{2\pi} \frac{d}{d\vartheta}\left[\operatorname{ch}\left(\frac{\psi-\vartheta}{2}\right) - \operatorname{ch}\left(\frac{\psi}{2}\right)\right]\sin n\vartheta\, d\vartheta \tag{5.3}$$

where account has been taken of the range of the upper surface inlet and the particular shape of the thin airfoil. Noting further that $V_0(\psi)$ is constant, the expression for the coefficients B_n may be written

$$B_n = -\frac{\gamma}{n\pi}\int_{\pi}^{2\pi}\cos\vartheta\,\sin n\vartheta\,d\vartheta$$

$$+\frac{\gamma}{4n\pi^2}\frac{V_a}{U_o}\int_{\pi/4}^{3\pi/4}d\psi\int_{\pi}^{2\pi}\frac{d}{d\theta}\left[\operatorname{ctn}\left(\frac{\psi-\vartheta}{2}\right)-\operatorname{ctn}\left(\frac{\psi}{2}\right)\right]\sin n\vartheta\,d\theta \tag{5.4}$$

Carrying out the detailed evaluations for the first two coefficients gives

$$B_1 = \frac{\sqrt{2}}{4\pi^2}\gamma\frac{V_a}{U_o}\left\{\log\left(\frac{\sqrt{2}+1}{\sqrt{2}-1}\right)-\pi\right\} \tag{5.5}$$

$$B_2 = \frac{2}{3\pi}\gamma \tag{5.6}$$

These particularly simple forms for these coefficients are due, not only to the convenient airfoil shape, but also to the symmetry and terminal angles for the uniform inlet.

Thus, to the second coefficient of the airfoil shape expansion, we may write down the aerodynamic coefficients for the airfoil with strong inlet,

$$C_L = 2\pi\left(\sin\alpha+\frac{2}{3\pi}\gamma\right)$$

$$+\frac{V_a}{U_o}\left\{+\log\left(\operatorname{ctn}\tfrac{\pi}{8}\right)+\frac{\gamma}{2\sqrt{2}\pi}\left[\log\left(\frac{\sqrt{2}+1}{\sqrt{2}-1}\right)-\pi\right]\right\} \tag{5.7}$$

$$C_D = \frac{\pi}{4}\frac{V_a}{U_o} \tag{5.8}$$

$$4C_M = -\left(2\pi + \frac{1}{4}\frac{V_0}{U_0}\right)\sin\alpha - \frac{V_0}{U_0}\left\{\sqrt{2} + \left(\frac{1}{3} - \frac{\sqrt{2}}{4}\right)J + \frac{\sqrt{2}\,J}{4\pi}\log\left(\frac{\sqrt{2}+1}{\sqrt{2}-1}\right)\right\}$$

$$+ \frac{1}{4}\left(\frac{V_0}{U_0}\right)^2\left\{-\log\left(\cot\beta/2\right) + \frac{J}{2\sqrt{2}\,\pi}\left(\pi - \log\left(\frac{\sqrt{2}+1}{\sqrt{2}-1}\right)\right)\right\} \qquad (5.9)$$

When the airfoil shape is reduced to a flat plate, by setting the thickness to zero, we recover the results given by equations (2.16)-(2.18).

6. JOUKOWSKI AIRFOIL WITH STRONG INLET FLOW

The thin airfoil analysis given in Sections 3, 4, and 5, while capable of dealing with any airfoil contour, is restricted to small perturbations and hence is limited in its capability of demonstrating the inherent limits of the strong inlet airfoil theory. For this purpose we shall develop the theory of the Joukowski airfoil with strong inlet flow in a similar manner to its conventional theory.

Force and Moment Coefficients

In presenting the properties and performance of a Joukowski airfoil with strong distributed suction, the analysis will not be given in detail but will be understood to proceed in the same general manner as that utilized in Sections 3 - 5. The mapping proceeds in a similar way, starting from a circle in the z plane as shown in figure 4; the values m, b, and δ determine the thickness and camber of the airfoil. The auxiliary angle β is also found convenient in the analysis but is, of course, not independent of the other parameters. For the examples to be discussed,

the values of the parameters were chosen

$$m = 0.4$$

$$b = 0.695$$

$$\delta = 50^{\circ}$$

$$\beta = 17.84^{\circ}$$

so as to obtain an airfoil having the properties

$$\text{camber} = 0.172 ,$$

$$\frac{\text{maximum thickness}}{\text{chord}} = 0.40 .$$

For the first set of examples, the general value of inlet to free stream velocity was taken to be $V_0/U_0 = 1.0$; larger values are described subsequently. Figures 5 and 6 show the lift coefficient and moment coefficient versus angle of attack for a range of inlet sizes, all symmetrically located. The values of $\psi_2 - \psi_1$ represent the extent of the inlet as described in the circle plane. The moment coefficient is substantially influenced, largely because the downstream edge of the inlet approaches the training edge of the wing quite rapidly as the extent of the inlet is increased. The curves for $\psi_2 - \psi_1 = 0$ represent base values for the airfoil without inlet.

The next set of results, figures 7 and 8, show the results of locating the inlet in an asymmetric manner, keeping the inlet size and velocity ratio constant. The position of the inlet is indicated by $\frac{1}{2}(\psi_1 + \psi_2)$, which is the angle of the midpoint of the inlet in the circle plane. All positions

shown are ahead of the midchord at a location favorable for actual installation. The angle of 110° is probably the farthest forward point that is practical for this inlet. The lift coefficient approaches that of the conventional airfoil as the inlet moves forward, again because the effect on circulation becomes smaller as the inlet becomes more remote from the trailing edge. The moment coefficient changes surprisingly little as the inlet position is altered. There is some noticeable change in the slope of the moment curve and some trend toward lower moments for very far forward positions of the intake. The gross result is a marked increase in moment coefficient over the conventional airfoil, similar to that shown in figure 6.

Detailed calculations were made for a variety of non-uniform inlet velocity distributions which ingested the same amount of fluid per unit time. Triangular (or linear) velocity distributions of rather extreme distortion, parabolic velocity distribution, with the velocity peaks and the center and at the edges, were used. The results demonstrated surprisingly small effect of lift or moment over the entire range of angles of attack.

The results of calculations of gross airfoil characteristics suggest that they are sensitive to the total intake flow, mildly sensitive to the location of the inlet, but quite insensitive to non-uniform distribution of inlet velocity.

Details of the Flow Field

The complex potential follows directly from equations (2. 3),

(2.4) and is appropriately written for the Joukouski airfoil as

$$w = \left\{ z e^{-i\alpha} + 1/z e^{-i\alpha} + 2i \sin(\alpha+\beta) \log z \right\}$$
$$+ i \log z \cdot \frac{1}{2\pi} \int_{\psi_1}^{\psi_2} \frac{\gamma_0}{U_0} \operatorname{ctn}\left(\frac{\psi+\beta}{2}\right) d\psi$$
$$- \frac{1}{\pi} \int_{\psi_1}^{\psi_2} \frac{\gamma_0}{U_0} \left\{ \log(z - e^{i\psi}) - \log z \right\} d\psi - \frac{1}{2\pi} \int_{\psi_1}^{\psi_2} \frac{\gamma_0}{U_0} \log z \, d\psi \qquad (6.1)$$

where $w = \frac{\tilde{w}(z)}{U_0 \, c/4}$, and, as before, the z plane is the unit circle plane. The first term of equation (6.1) is the familiar complex potential for the uniform flow past a unit circular cylinder with an angle of attack α and circulation. The second term is the complex potential of a circulation about a unit circular cylinder, induced by the intake flow, required to satisfy the Kutta condition. The third term is the complex potential of the continuous sum of source-sink pairs, distributed on the periphery of the unit circle in the region $\psi_1 \leq \psi \leq \psi_2$. The last term of the equation (6.1) is the complex potential of the sum of the sinks at the origin of the z plane, required to maintain the circular cylinder as a streamline.

The dimensionless stream function ψ is obtained from (6.1) by letting $z = re^{i\vartheta}$ and determining the imaginary part of w . Explicitly, the stream function is

$$\Psi = (r - 1/r)\sin(\vartheta-\alpha) + 2\sin(\alpha+\beta)\log r$$
$$+ \frac{1}{2\pi}\log r\int_{\psi_1}^{\psi_2}\frac{V_0}{U_0}\operatorname{ctn}\left(\frac{\psi+\beta}{2}\right)d\psi + \frac{1}{\pi}\int_{\psi_1}^{\psi_2}\frac{V_0}{U_0}\tan^{-1}g(r,\vartheta,\psi)\,d\psi$$
$$- \frac{\vartheta}{2\pi}\int_{\psi_1}^{\psi_2}\frac{V_0}{U_0}\,d\psi \qquad (6.2)$$

where

$$g(r,\vartheta,\psi) = \frac{2\cos\vartheta\,(r\sin\psi - \sin\vartheta)}{r^2 - 1 - 2\sin\vartheta\,(r\sin\psi - \sin\vartheta)} \qquad (6.3)$$

In equation (6.2), it is implied that the numerical values of the angle of attack, α, and β, which is a measure of Joukowski airfoil camber, are known and the functional form of suction velocity $V_0(\psi)$ is prescribed in the z plane over a region $\psi_1 \leq \psi \leq \psi_2$ on the unit circle. When a numerical value for the stream function Ψ is prescribed, one can generate the corresponding streamline in the z plane as follows. Assign a set of values for ϑ in the range $(0, 2\pi)$, and then for each value of ϑ determine the corresponding value of r satisfying equation (6.2). Once the coordinates (r, ϑ) of a streamline in the z - plane are determined, then the coordinates of the corresponding streamline in the airfoil plane, the ζ plane, are determined by using the transformation given in equation (2.5). The details of this method for streamline coordinate determination will be illustrated with a representative example.

Consider a Joukowski airfoil with a camber of 0.06 and maximum thickness-to-chord ratio of 0.125. The corresponding values of the airfoil parameters b and β are 0.9 and 6.84°, respectively. Let the angle of attack α be 0°, and choose the suction velocity to be constant in the region $60^{\circ} \leq \psi \leq 120^{\circ}$. By taking $V_0(\psi) = V_0 = \text{constant}$, (6.2) can be rewritten as

$$\frac{1}{(\pi/2 - \psi_1)} \int_{\psi_1}^{\pi/2} \tan^{-1} g(r, \vartheta, \psi)\, d\psi$$

$$- \left\{ \frac{1}{\pi/2 - \psi_1} \left[\frac{\Psi}{2V_0/U_0} - K_2 (r - 1/r) - K_1 \log r \right] + \vartheta \right\} = 0 \qquad (6.4)$$

where

$$K_1 = \frac{2\pi}{V_0/U_0} \sin(\alpha + \beta) + \log \left| \frac{\sin \frac{1}{2}(\pi - \psi_1 + \beta)}{\sin \frac{1}{2}(\psi_1 + \beta)} \right|$$

$$K_2 = \frac{\pi}{V_0/U_0} \sin(\vartheta - \alpha) \qquad (6.5)$$

As indicated already for specified numerical values of Ψ, V_0, and ϑ, the equation (6.4) is to be solved for r. The numerical method which is suitable for this purpose is the well-known iterative Newton-Raphson technique. Let us denote the left hand side of equation (6.4) as $F(r)$. For the Newton-Raphson method to converge to a solution r, a close approximation to it must first be determined. This was done by assigning a set of values for $r > 1.0$ and then evaluating $F(r)$.

When computations for two successive values of r lead to a sign change in the value $F(r)$, the desired solution is bracketed. With this approximate solution as the initial value for r, the Newton-Raphson iterations continued until the absolute value of relative error between two successive iterations is less than or equal to 10^{-5}. The definite integrals appearing in $F(r)$ and $dF(r)/dr$ that are utilized in this iterative scheme are evaluated numerically by using Simpson's rule with $\Delta\psi = 1^{\circ}$. When a solution pair (r, ϑ) is obtained on the streamline, it is possible to progress along that streamline by choosing increments of about 4° or less in ϑ and successively computing the corresponding new value r by using the last computed value r as its initial value in the iteration procedure.

Further remarks on the numerical integration are appropriate at this point. Both $F(r)$ and $dF(r)/dr$ contain the integral

$$I(r) \equiv \frac{1}{(\pi/2 - \psi_1)} \int_{\psi_1}^{\pi/2} \tan^{-1} g(r, \vartheta, \psi)\, d\psi \quad .$$

The integrand $\tan^{-1} g(r, \vartheta, \psi)$ is multi-valued. The Newton-Raphson method requires that $I(r)$ be continuous in r except possibly for $r = 1.0$. Furthermore, since $I(r)$ is an average angle, it will be convenient if it remains in the range $(0, 2\pi)$. This, in turn, will require $\tan^{-1} g(r, \vartheta, \psi)$ be continuous in ψ during numerical integration and also be in the range $(0, 2\pi)$. To fulfill these set requirements, ex-

haustive numerical calculations were made to find a way of assigning values to $\tan^{-1} g(r, \vartheta, \psi)$ based on the algebraic signs of the numerator g_x and denominator g_y of $g(r, \vartheta, \psi)$ in equation (6.3). In this type of computation, it is necessary first to assign values for ϑ in the range $(0, 2\pi)$, and then for each value of ϑ to assign values for r in the range $0 \leq r \leq r_{max}$. Then, for each (ϑ, r) combination, numerical values of $\tan^{-1} g(r, \vartheta, \psi)$, g_x, and g_y are computed as ψ is varied in the range from $\pi/3$ to $\pi/2$. Here, r_{max} is an arbitrary radius of interest in the z- plane. For this study, $r_{max} = 3.2$. The results of this study are summarized in Table I. The entries in this table are to be interpreted as follows: when $0° \leq \vartheta \leq 90°$, $\tan^{-1} g(r, \vartheta, \psi)$ will vary in 2nd, 3rd, and 4th quadrants if $\tan^{-1} g(r, \vartheta, \psi)$ is determined as based on the signs of g_x and g_y when $0 \leq r \leq 1$ and if $\tan^{-1} g(r, \vartheta, \psi)$ is determined as based on the signs of $-g_x$ and $-g_y$ when $1 < r \leq 3.2$.

For the flow field calculations the airfoil having the shape shown in figure 9 was chosen, having a 6 percent camber and a thickness/chord radio of 0.125. This shape was obtained by using the parameter values $m = 0.15172$, $b = 0.89895$, $\delta = 51.75°$, and $\beta = 6.84°$. Computations were made on a digital computer, and figures 10, 11, and 12 present typical streamlines in the airfoil plane for the ratios of suction velocity to the free stream velocity, V_0/U_0, of 6, 14, and 15, respectively.

When $V_0/U_0 = 6.0$, a moderate suction to free stream velocity ratio, there are three stagnation points, labeled S_1, S_2, and S_3 on figure 10. S_1 is the stagnation point that was originally at the leading

TABLE I

	$0^\circ \le \theta \le 90^\circ$	$90^\circ < \theta \le 180^\circ$	$180^\circ < \theta \le 270^\circ$	$270^\circ < \theta < 360^\circ$
$\tan^{-1} g(r_1, \theta, \psi)$	2 , 3 , 4	1 , 2 , 3	1 , 2 , 3	1 , 2 , 3
$0 \le r_1 \le 1.0$	g_x , g_y	g_x , g_y	$-g_x$, $-g_y$	g_x , g_y
$1.0 < r_1 < 3.2$	$-g_x$, $-g_y$	$-g_x$, $-g_y$		

edge of the airfoil when $V_0/U_0 = 0$. S_2 is the stagnation point that was originally at the aft edge of the inlet. The trailing edge stagnation point , S_3 , is fixed by the imposed Kutta condition. As the suction to free stream velocity ratio, V_0/U_0 , is increased the stagnation points S_1 and S_2 move towards the trailing edge of the airfoil. Figure 11 shows the streamlines for $V_0/U_0 = 14.0$, where in this figure the stagnation point S_2 is now on the underside of the airfoil. The trailing edge stagnation point S_3 remains fixed.

Figure 12 shows streamlines for $V_0/U_0 = 15.0$. For this suction to free stream velocity ratio, stagnation points S_1 and S_2 are no longer on the airfoil surface. One of the stagnation points is in the flow field labeled as S_1 , and the other is in the interior of the airfoil and is not shown in the figure. It is interesting to note that with this inlet flow, streamlines originating above the airfoil go around and underside of the airfoil, around the leading edge, and finally enter the inlet. In figure 10, the streamlines leave the stagnation point S_3 , but in figures 11 and 12 the streamlines approach the stagnation point S_3 . Under these conditions, the trailing edge has, in fact, become a leading edge.

From figures 10 - 12 it is clear that the location of stagnation points S_1 and S_2 depend rather sensitively on the value of the suction to free stream velocity ratio, V_0/U_0 . Considerable information regarding the structure of the flow field may be obtained by investigating the dependence of the locations on these three stagnation points upon the value

of V_0/U_0 . Consequently, the details of this dependence will be investigated.

A stagnation point in a flow field is characterized by the vanishing of the complex velocity. When the stagnation points lie on the airfoil surface, that is, on the unit circle in the z - plane, the angle ϑ satisfies the equation

$$2\pi \sin(\vartheta-\alpha) - V_0/U_0 \log\left\{\frac{\cos\frac{1}{2}(\psi_1+\vartheta)}{\sin\frac{1}{2}(\psi_1-\vartheta)}\right\} + 2\pi \sin(\alpha+\beta)$$

$$+ V_0/U_0 \log\left|\frac{\cos\frac{1}{2}(\psi_1-\beta)}{\sin\frac{1}{2}(\psi_1+\beta)}\right| = 0 \qquad (6.6)$$

On the other hand, when the stagnation points are off the airfoil surface, the following pair of equations must be satisfied.

$$\frac{\pi}{V_0/U_0}(r-1/r)\cos(\vartheta-\alpha) - (\pi/2-\psi_1)$$

$$- \tan^{-1}\left\{\frac{-2\cos\psi_1(\sin\psi_1 - r\sin\vartheta)}{r^2-1+2\sin\psi_1(\sin\psi_1 - r\sin\vartheta)}\right\} = 0$$

$$\frac{\pi}{V_0/U_0}(r+1/r)\sin(\vartheta-\alpha) - \frac{1}{2}\log\left|\frac{r^2+1+2r\cos(\vartheta+\psi_1)}{r^2+1-2r\cos(\vartheta-\psi_1)}\right| \qquad (6.7)$$

$$+ \frac{2\pi}{V_0/U_0}\sin(\alpha+\beta) + \log\left|\frac{\cos\frac{1}{2}(\psi_1-\beta)}{\sin\frac{1}{2}(\psi_1+\beta)}\right| = 0 .$$

The equation (6.6) is restricted to values of ϑ for which

$$\frac{\cos\frac{1}{2}(\psi_1+\vartheta)}{\sin\frac{1}{2}(\psi_1-\vartheta)} > 0$$

This is equivalent to saying that ϑ cannot take values in the range from ψ_1 to $\pi - \psi_1$, that is, there cannot be any stagnation points in the inlet region of the airfoil.

When $\vartheta = -\beta$, the equation (6.6) is satisfied regardless of the value of suction to free stream velocity ratio, V_o/U_o. Thus, the stagnation point S_3 remains stationary at the trailing edge.

When $V_o/U_o = 0$, the equation (6.6) reduces to

$$4\pi \sin \tfrac{1}{2}(\vartheta+\beta) \cos \tfrac{1}{2}(\vartheta - 2\alpha - \beta) = 0 \qquad (6.8)$$

and there are two stagnation points at $\vartheta = \pi + 2\alpha + \beta$ and $\vartheta = -\beta$. These are the familiar stagnation points in the z-plane for the uniform flow past the airfoil, the leading and the trailing edge stagnation points.

For non-zero values of suction to free stream velocity ratio, equation (6.6) is solved for ϑ by using the Newton-Raphson method. When V_o/U_o is slightly greater than zero, there are three solutions of the equations (6.6), two of which are the leading and trailing edge stagnation points. The third stagnation point appears slightly to the right of the downstream edge of the inlet region on the airfoil. As the suction to free stream velocity ratio increases, the latter and the leading edge stagnation points move toward the trailing edge of the airfoil, as shown in figure 13 in the z- plane. The loci of these two stagnation points merge and separate for $V_o/U_o = 14.1125$ on the underside of the airfoil.

For $V_o/U_o > 14.12$, the loci are determined by solving simultane-

ously the pair of equations (6.7) for r and ϑ. The method of solution is again the Newton-Raphson method. The loci that merged on the periphery of the unit circle in the ζ-plane separate in opposite radial directions. One locus proceeds to the origin of the ζ plane and the other proceeds to infinity. Geometrically, these two loci are images.

It is to be noted that once loci of stagnation points are available in the ζ-plane, such as figure 13, or corresponding figure in airfoil plane, then streamlines as shown in figures 10 - 12 can be sketched readily.

7. CONCLUDING REMARKS

An extension of conventional thin-airfoil theory has been developed which is capable of calculating two-dimensional airfoil characteristics for wings having an arbitrary inlet on the upper surface with large inlet velocities. The importance of thin-wing linearization with respect to a flow field in which both free stream and inlet velocities may be large, is clearly demonstrated by the results. Results from the same analysis permit calculation of the flow field and pressure distribution and, particularly in the neighborhood of the inlet, this is not possible by other techniques.

In order to examine the limitations of the calculation, with regard to physical reality rather than to accuracy of the approximate analysis, the theory of the Joukowski airfoil was extended to include an arbitrarily located inlet on the upper surface of the airfoil having an arbitrarily distributed normal component of inlet velocity. The advantage of utilizing

the Joukowski theory for this exploration is that any unusual character of the results can in no way be attributed to the linearization.

The results for a Joukowski airfoil of particular shape showed that, with increasing mass flow into the inlet, the stagnation point which lies on the upper surface of the airfoil between the downstream edge of the inlet and the trailing edge of the airfoil, moves around the trailing edge of the airfoil onto the lower surface. Under these conditions, the flow approaches the trailing edge rather than leaving it, and consequently actually becomes a "leading edge." As a consequence, the Kutta condition is not longer applicable and assumptions of usual airfoil theory lose their physical validity. This occurs for a value of inlet velocity in the neighborhood of ten times the free stream velocity for the particular example treated. It is clearly a general result, however, and the phenomenon occurs well below the largest ratios of inlet to free stream velocity that are of interest. There is a legitimate question, moreover, whether the flow at the trailing edge gives a sufficiently strong singularity to dominate the flow up to the inlet velocity where the stagnation points coalesce at the trailing edge.

For very high values of inlet velocity, or for very low values of free stream speed, the structure of the flow field seems fairly clear. Under this circumstance the flow approaches the airfoil from below, separates from both leading and trailing edge, and flows into the inlet, leaving a finite separation zone at both leading and trailing edges. The

situations intermediate between this and the completely attached flow which we have described are not clear, and can only be clarified by some well-chosen experiments.

Finally, it should be mentioned that the entire process of flow into an upper surface inlet may be significantly different in three dimensions than in two. The inlets are either circular, for fan-in-wing configuration, or have spanwise extent not exceeding a wing chord. In either circumstance, the flow field is strongly three-dimensional and "leakage" into the region downstream of the intake may alter significantly the limits we have observed.

REFERENCES

1. Vogler, Raymond D., "Interference Effects of Single and Multiple Round or Slotted Jets on a VTOL Model in Transition," NASA TN D-2380 (1964).

2. Milne-Thomson, L. M., Theoretical Hydrodynamics, third edition, Macmillan Company, New York (1955), p. 209 ff.

3. Lamb, Sir Horace, Hydrodynamics, sixth edition, Cambridge University Press (1932), pp. 91-92.

4. Kármán, Th. von, Aerodynamic Theory, Vol. II, ed. W. F. Durand, Julius Springer (1935).

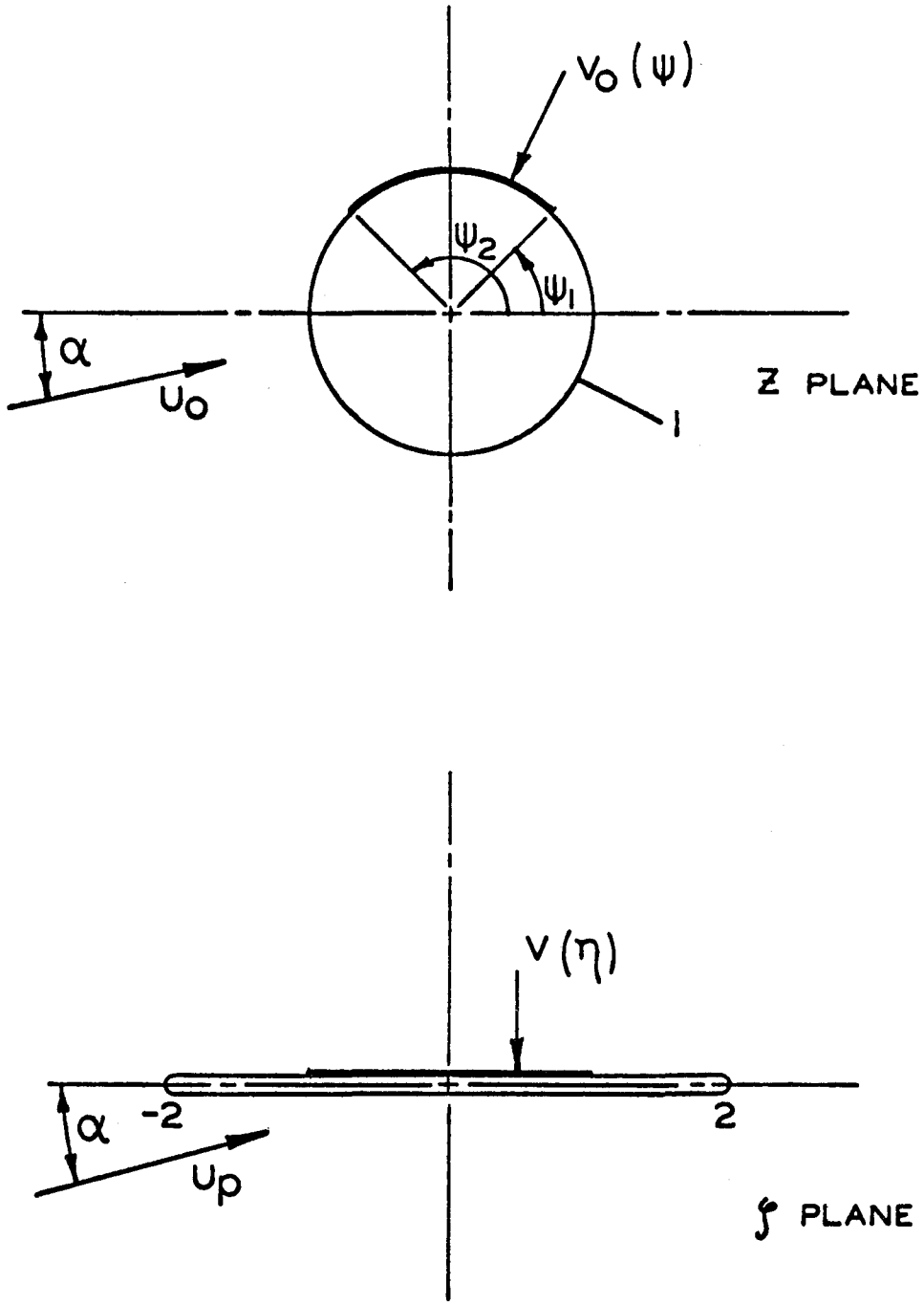

Figure 1. Definitions and Mapping for Circle Plane and Airfoil Plane.

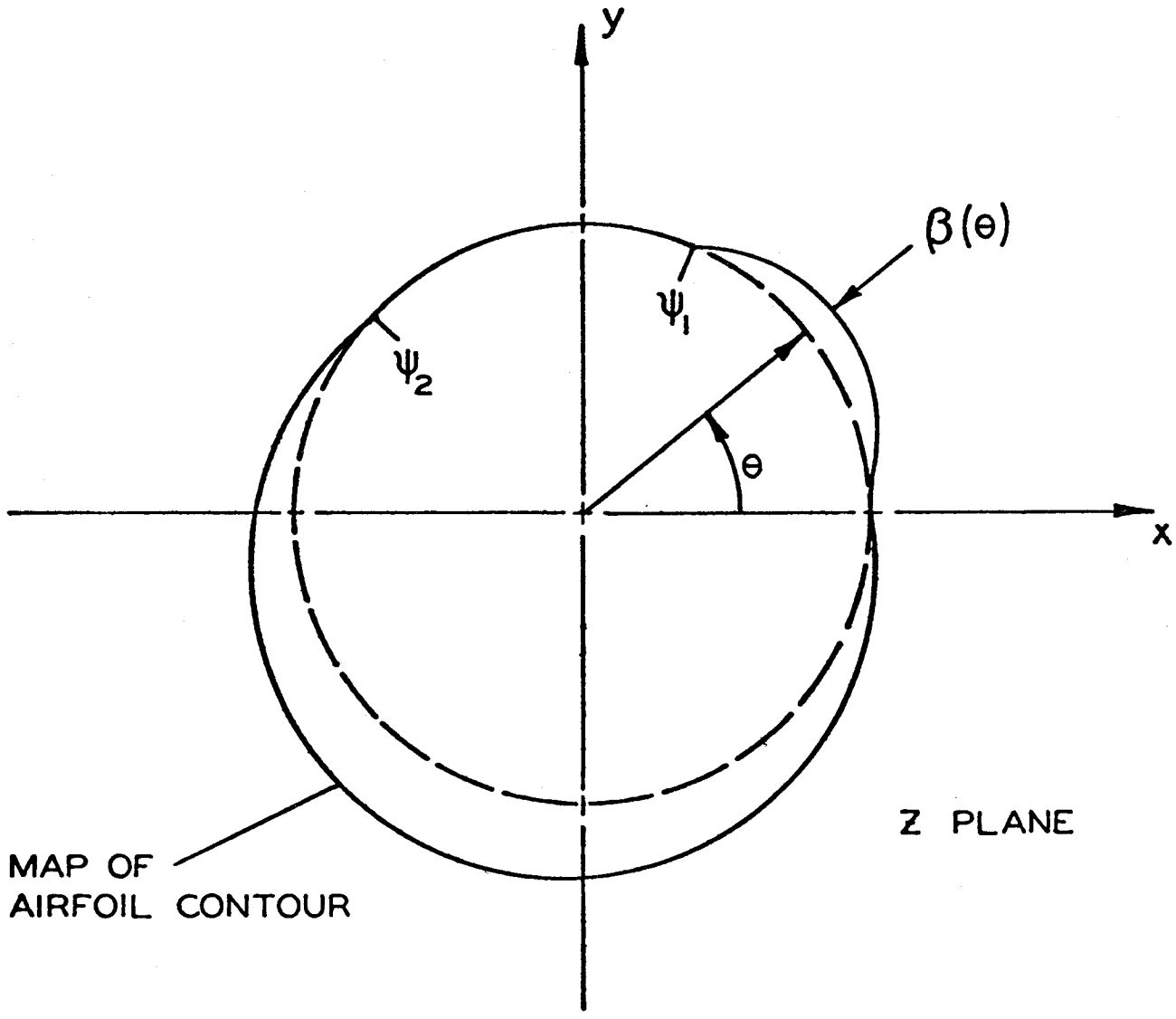

Figure 2. Mapping of Thin Airfoil in Circle Plane.

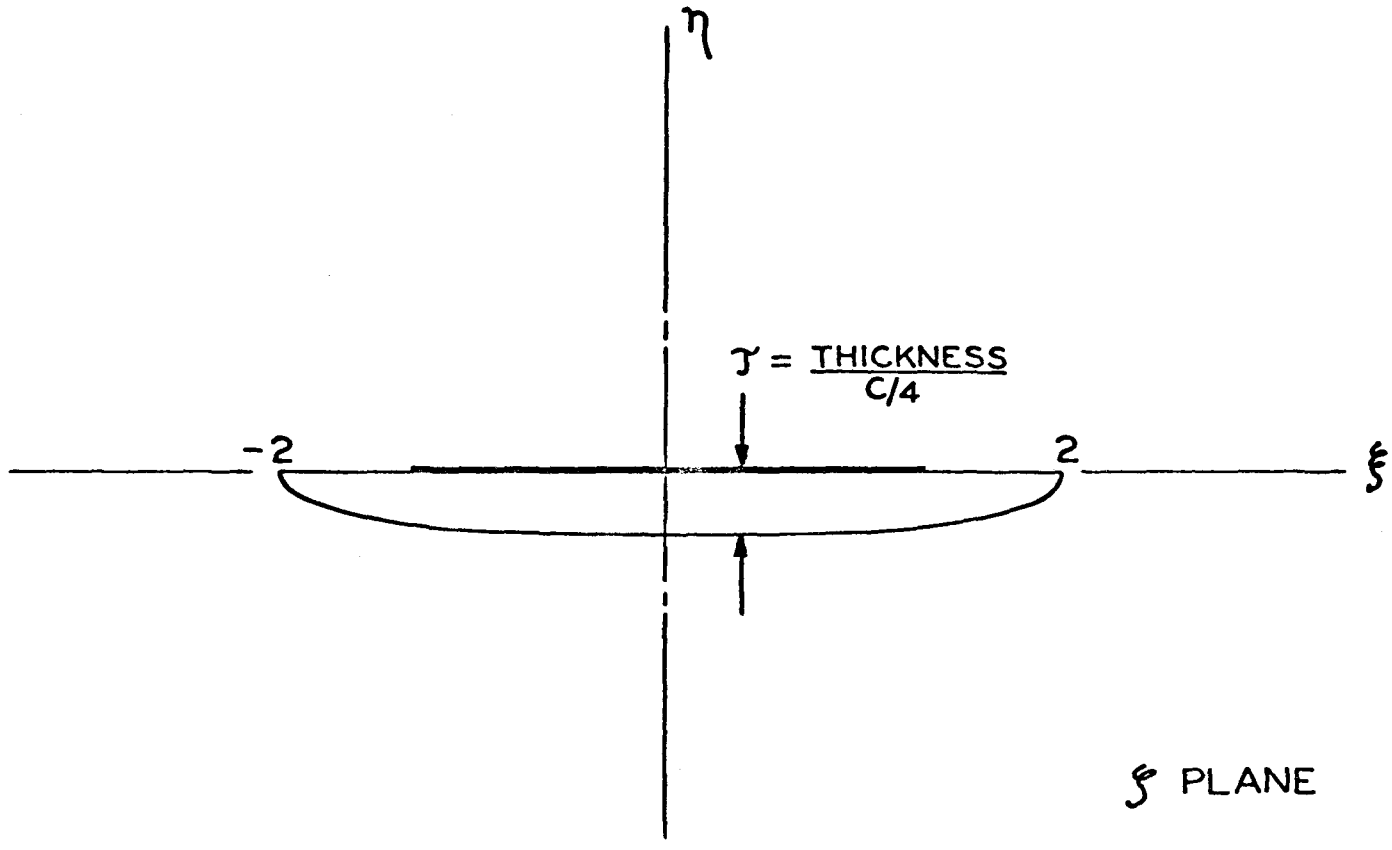

Figure 3. Airfoil Shape Used in Example.

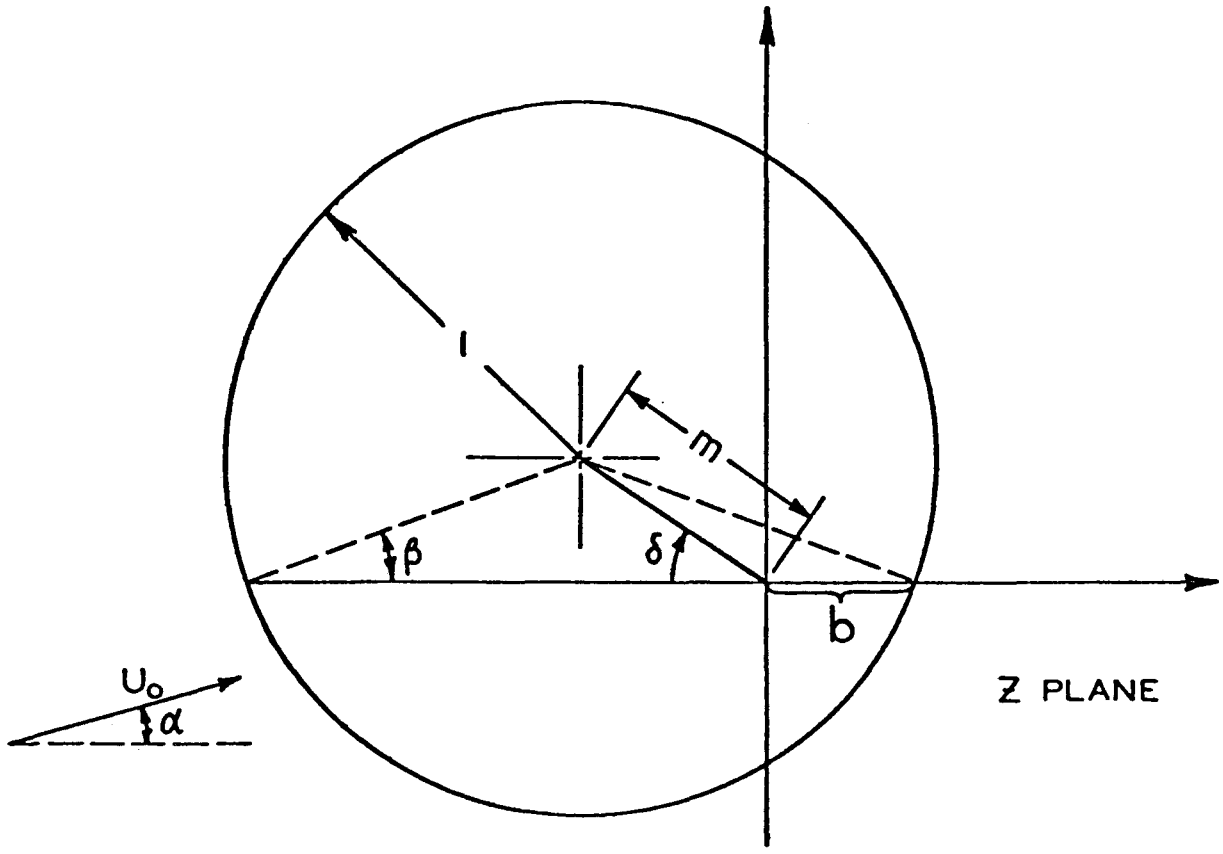

Figure 4. Mapping for Joukwski Airfoil.

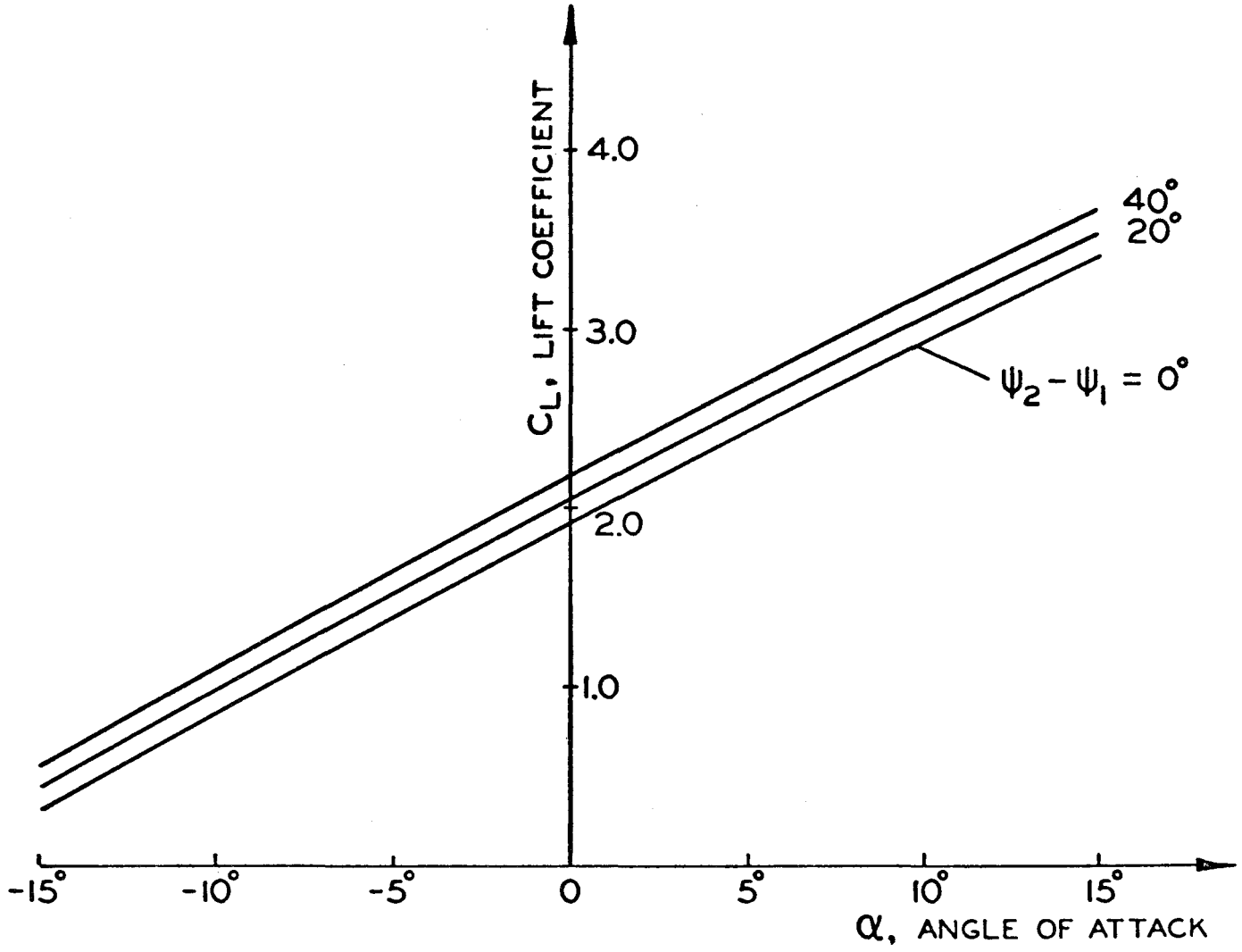

Figure 5. Lift Coefficients for Joukowski Airfoil with Symmetric Inlets, $V_o/U_o = 1.0$.

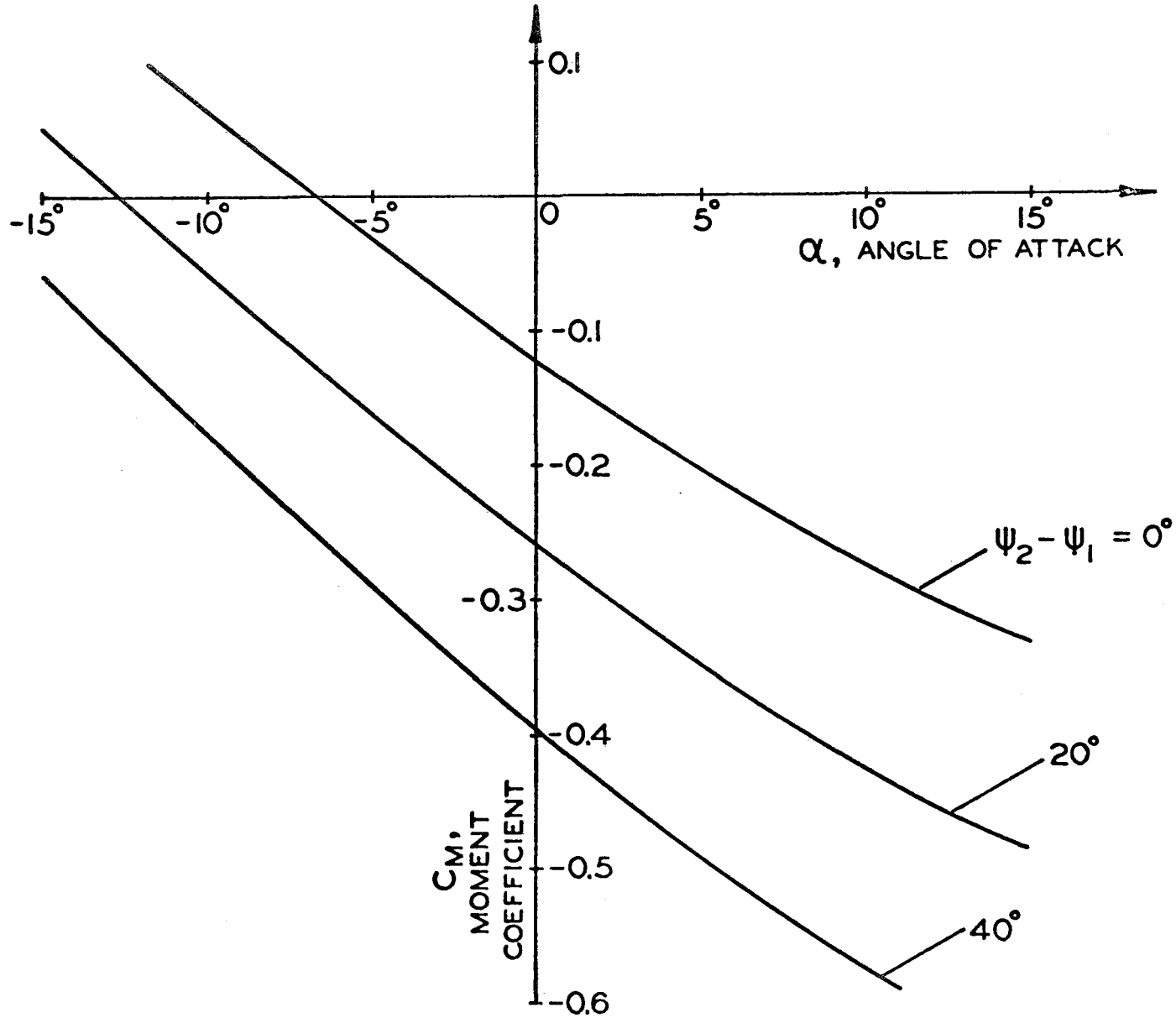

Figure 6. Moment Coefficient for Joukowski Airfoil with Symmetric Inlets, $V_o/U_o = 1.0$.

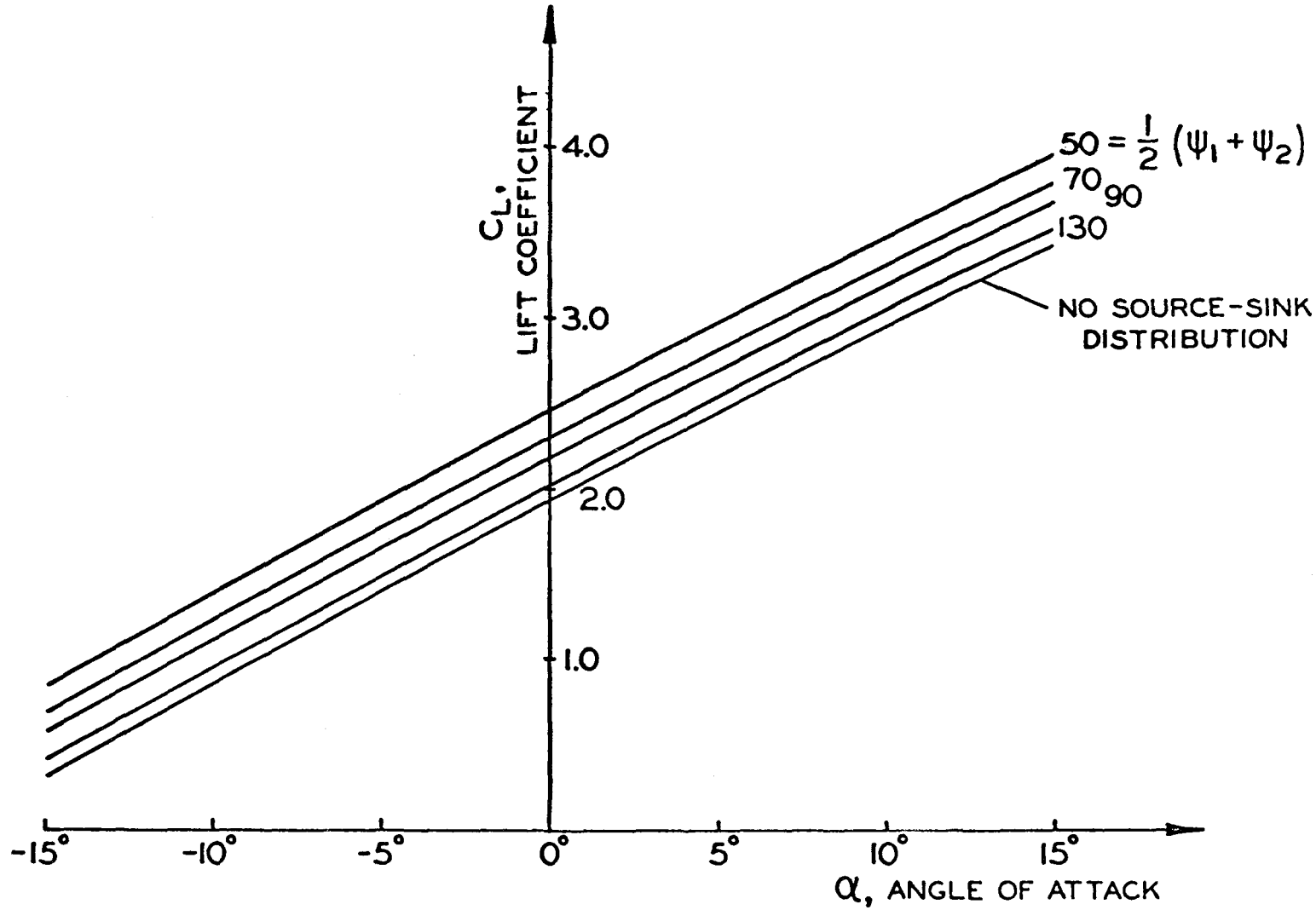

Figure 7. Lift Coefficients for Joukowski Airfoil with Asymmetric Inlets, $V_o/U_o = 1.0$, $\psi_2 - \psi_1 = 40^o$.

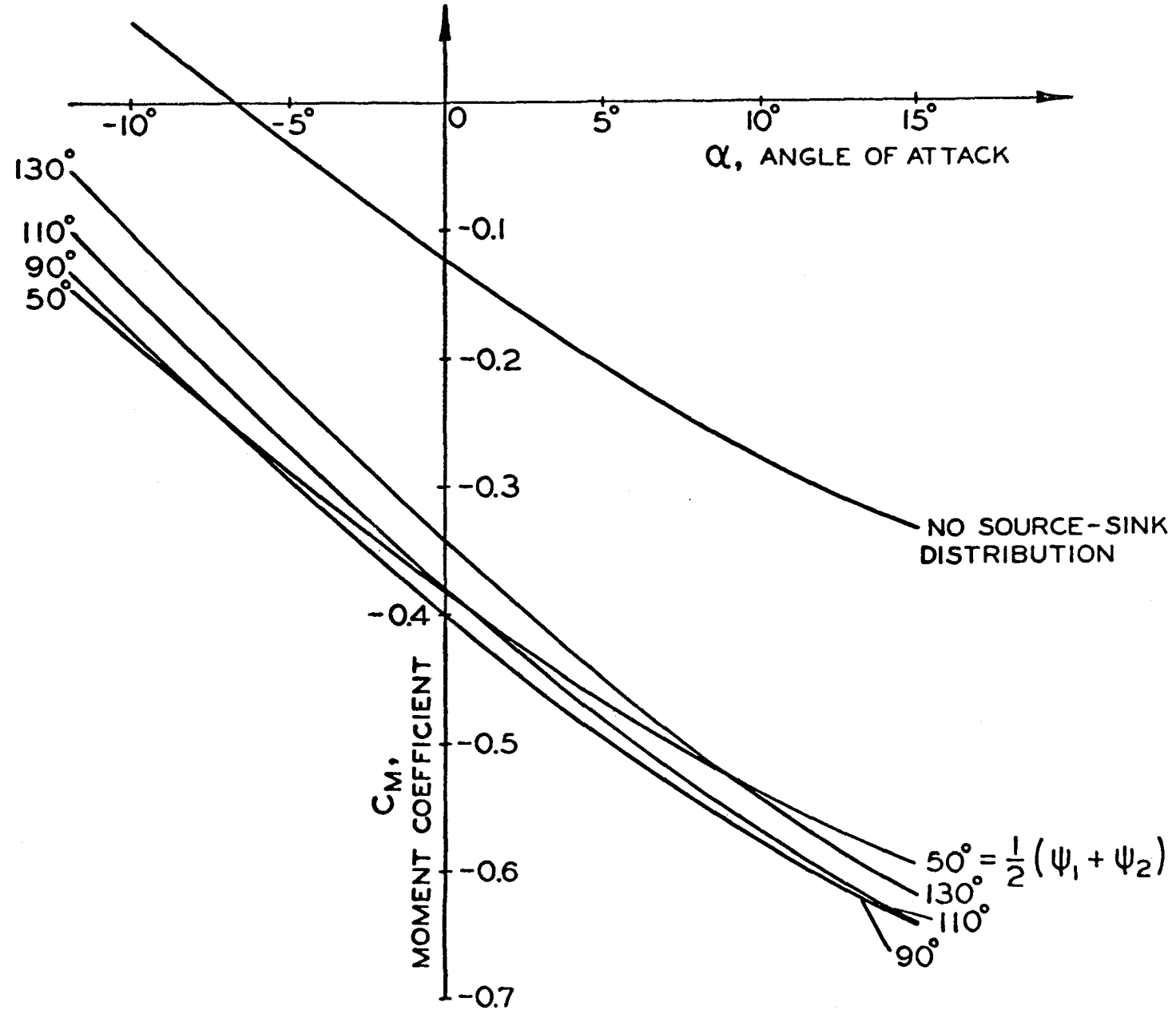

Figure 8. Moment Coefficients for Joukowski Airfoil with Asymmetric Inlets, $V_o/U_o = 1.0$, $\psi_2 - \psi_1 = 40^o$.

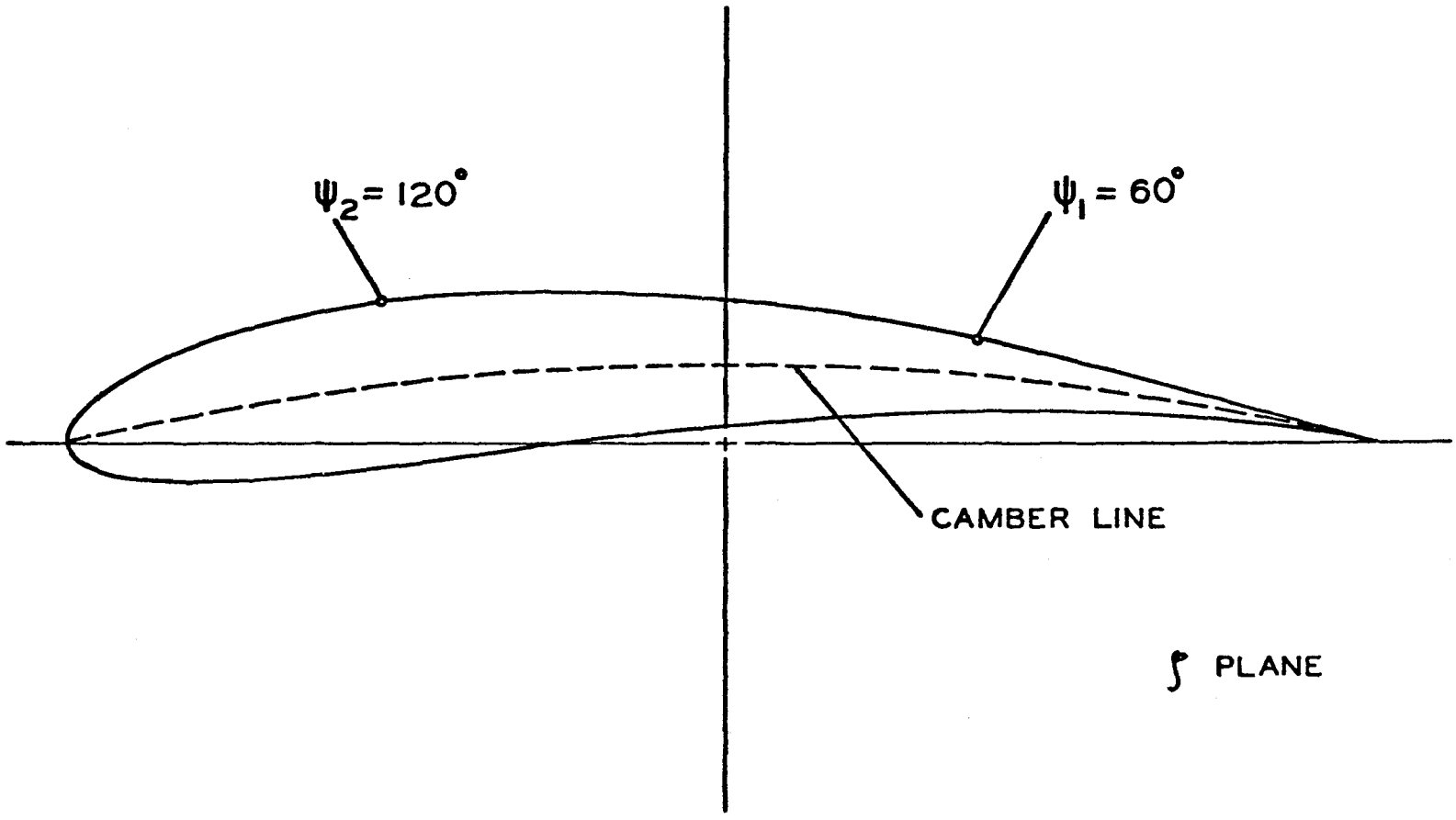

Figure 9. Joukowski Airfoil Used in Flow Pattern Calculations.

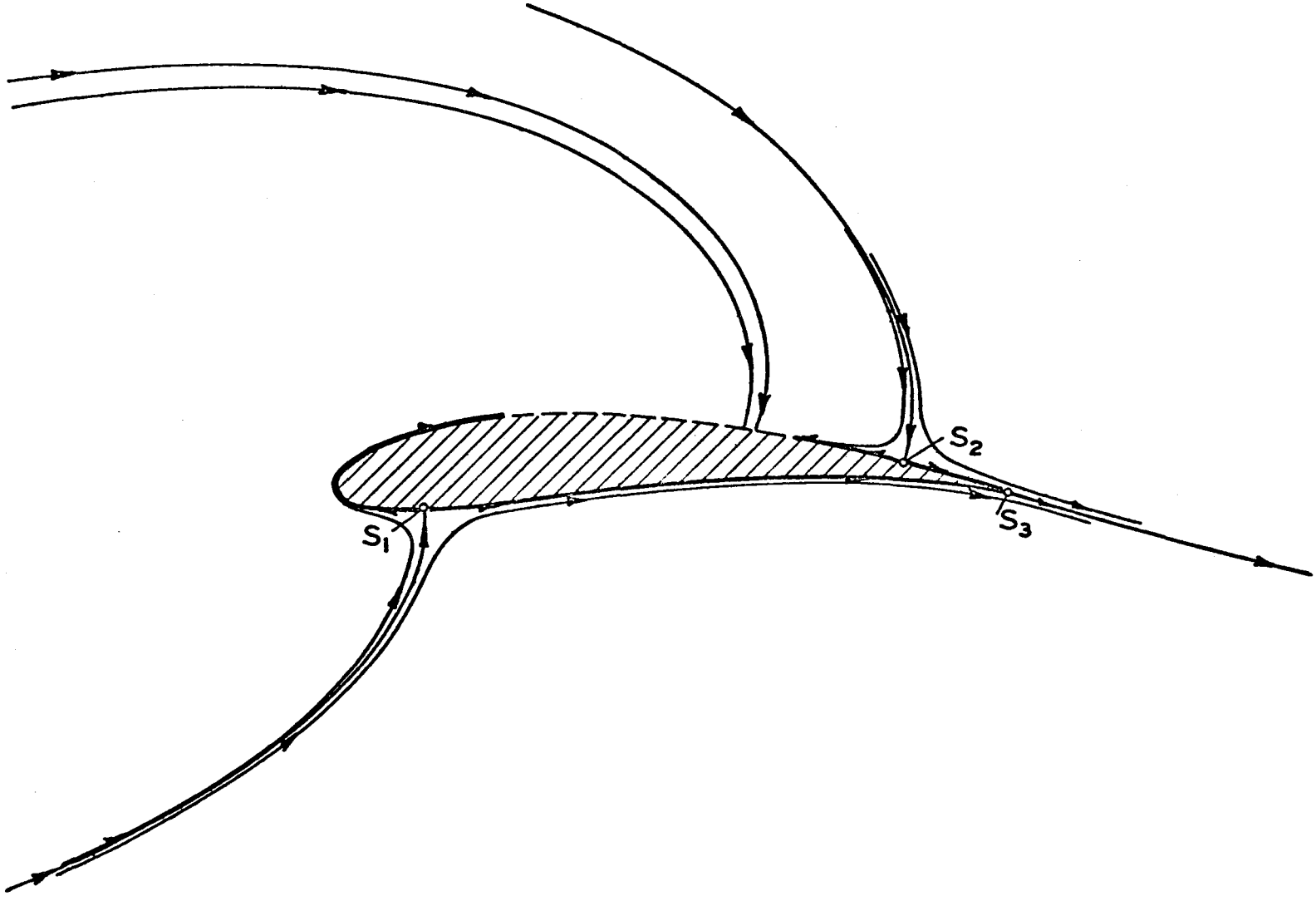

Figure 10. Streamline Pattern in Airfoil Plane, $V_\alpha / U_o = 6.0$.

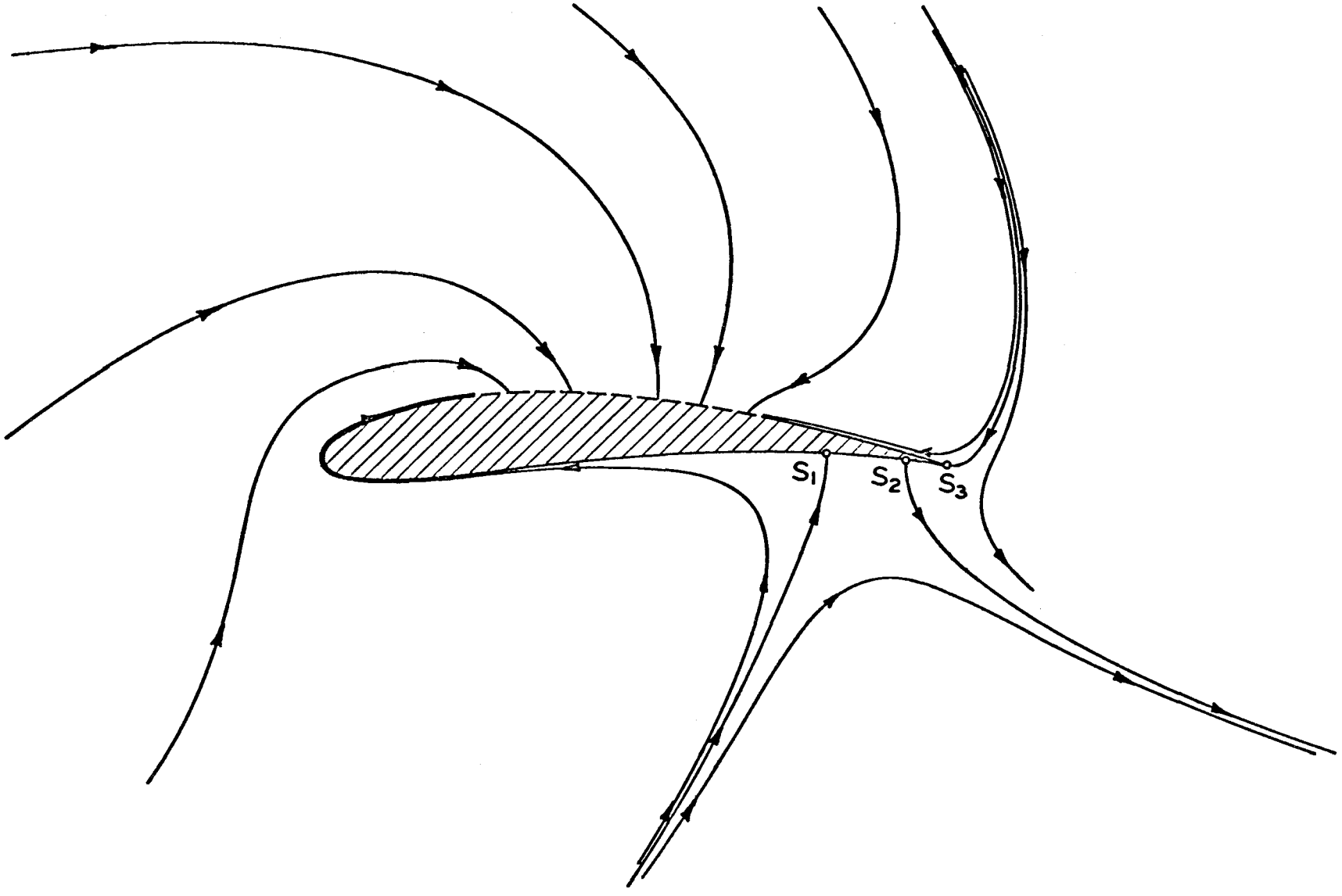

Figure 11. Streamline Pattern in Airfoil Plane, $V_o/U_o = 14.0$.

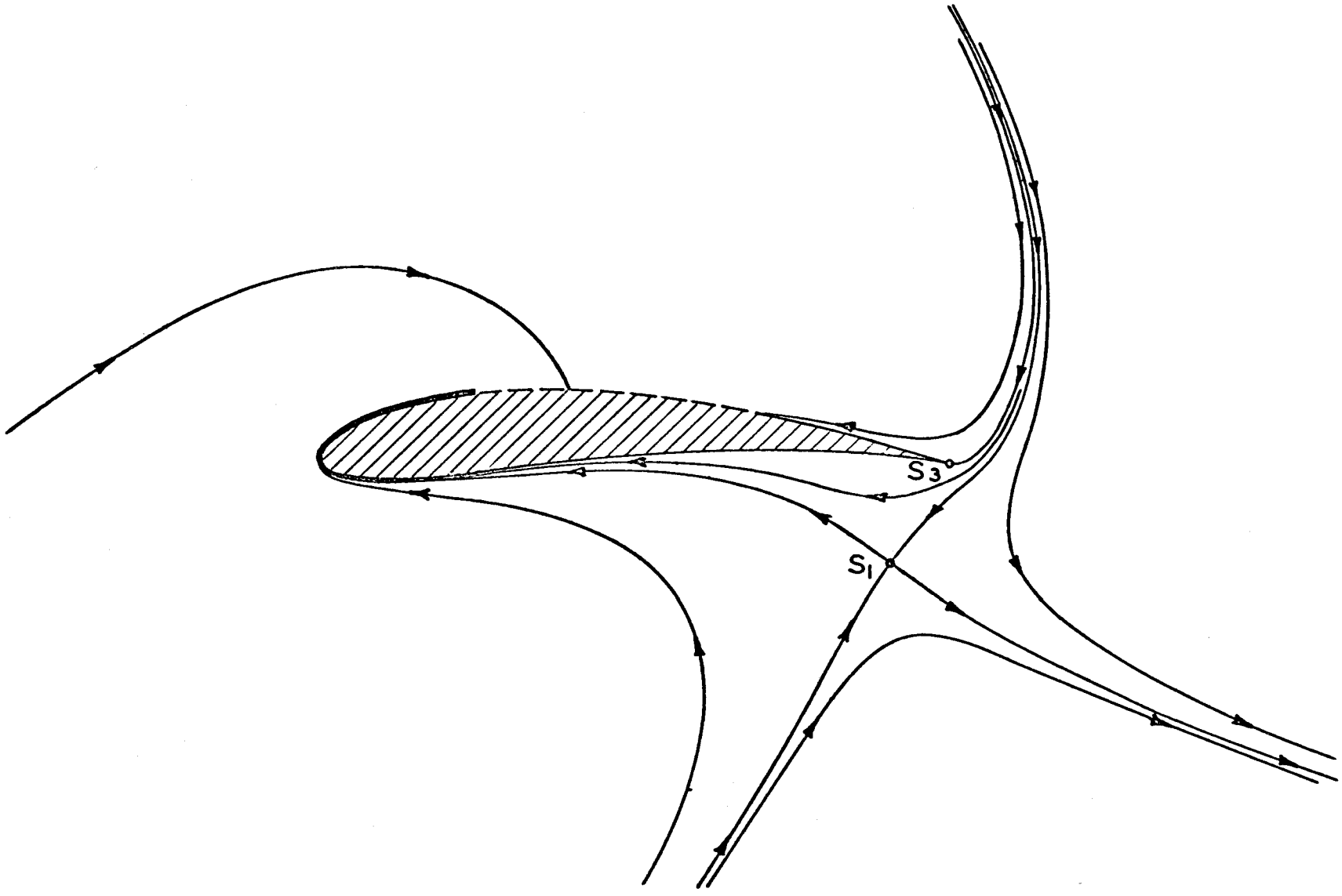

Figure 12. Streamline Pattern in Airfoil Plane, $V_o/U_o = 15.0$.

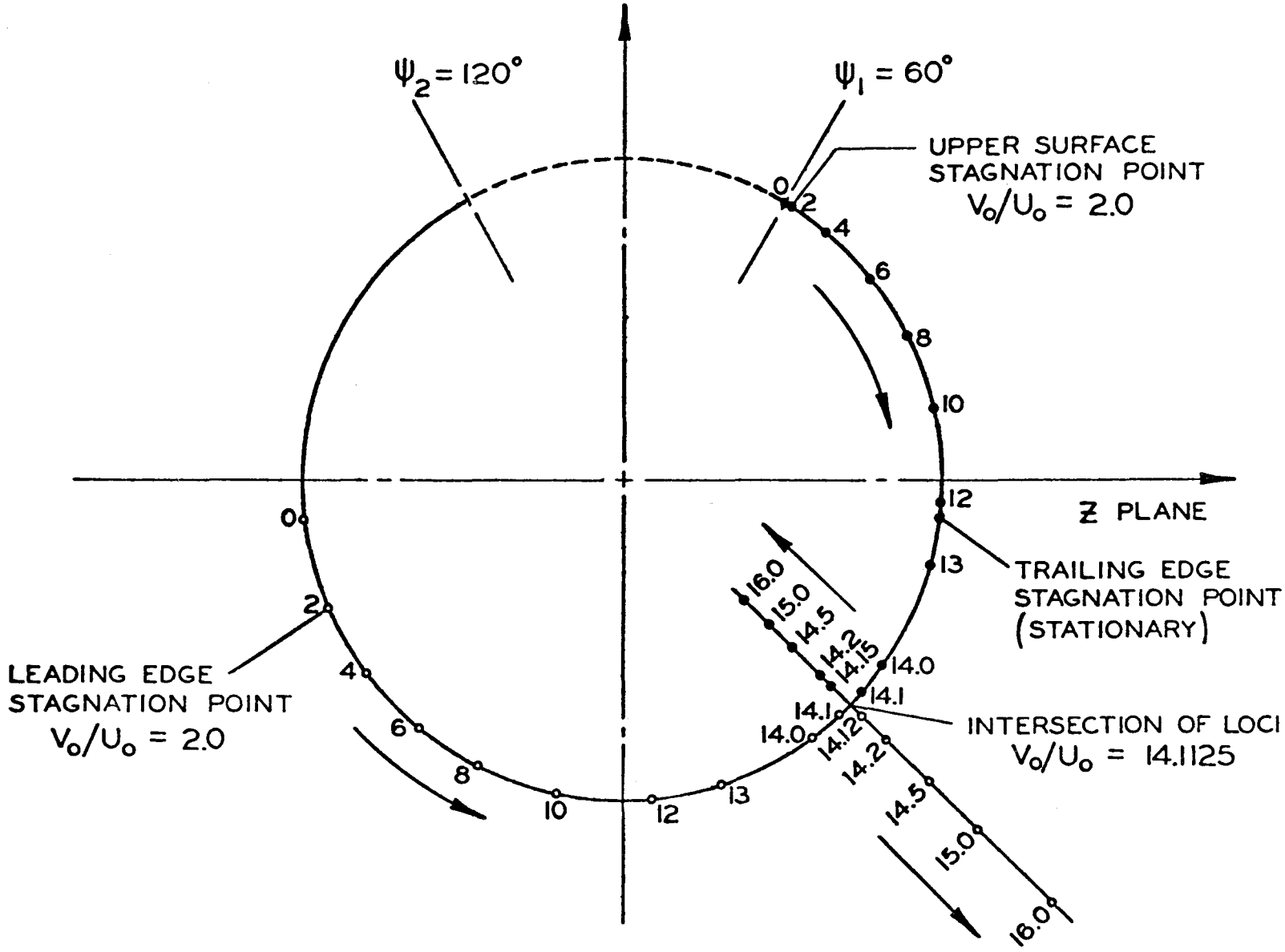

Figure 13. Loci of Stagnation Points in Circle Plane, Varying Value of V_o/U_o.

UNCLASSIFIED
Security Classification

DOCUMENT CONTROL DATA - R & D

(Security classification of title, body of abstract and indexing annotation must be entered when the overall report is classified)

1. ORIGINATING ACTIVITY (Corporate author)	2a. REPORT SECURITY CLASSIFICATION
California Institute of Technology Pasadena, California	Unclassified
	2b. GROUP

3. REPORT TITLE

A Theory of Two-Dimensional Airfoils with Strong Inlet Flow on the Upper Surface

4. DESCRIPTIVE NOTES (Type of report and inclusive dates)

Scientific, Final.

5. AUTHOR(S) (First name, middle initial, last name)

Sedat Serdengecti
Frank E. Marble

6. REPORT DATE	7a. TOTAL NO. OF PAGES	7b. NO. OF REFS
August 1970	60	4

8a. CONTRACT OR GRANT NO.	9a. ORIGINATOR'S REPORT NUMBER(S)
F33615-68-C-1013	
b. PROJECT NO. 7064	
c. DoD Element 61102F	9b. OTHER REPORT NO(S) (Any other numbers that may be assigned this report)
d. DoD Subelement 681307	ARL 70-0139

10. DISTRIBUTION STATEMENT

1. This document has been approved for public release and sale; its distribution is unlimited.

11. SUPPLEMENTARY NOTES	12. SPONSORING MILITARY ACTIVITY
TECH OTHER	Aerospace Research Laboratories (ARR) Wright-Patterson AFB Ohio 45433

13. ABSTRACT

The two-dimensional theory of airfoils with arbitrarily strong inlet flow into the upper surface was examined with the aim of developing a thin-airfoil theory which is valid for this condition. Such a theory has, in fact, been developed and reduces uniformly to the conventional thin-wing theory when the inlet flow vanishes. The integrals associated with the arbitrary shape, corresponding to the familiar Munk integrals, are somehwat more complex but not so as to make calculations difficult.

To examine the limit for very high ratios of inlet to free-stream velocity, the theory of the Joukowski airfoil was extended to incorporate an arbitrary inlet on the surface. Because this calculation is exact, phenomena observed in the limit cannot be attributed to the linearized calculation.

These results showed that airfoil theory, in the conventional sense, breaks down at bery large ratios of inlet to free-stream velocity. This occurs where the strong induced field of the inlet dominates the free-stream flow so overwhelmingly that the flow no longer leaves the trailing edge but flows toward it. Then the trailing edge becomes, in fact a leading edge and the Kutta condition is physically inapplicable. For the example in this work, this breakdown occurred at a ratio of inlet to free-stream velocity of about 10. This phenomena suggests that for ratios in excess of the critical value, the flow separates from the trailing edge and the circulation is dominated by conditions at the edges of the inlet.

DD FORM 1 NOV 65 1473

UNCLASSIFIED
Security Classification

14. KEY WORDS	LINK A		LINK B		LINK C	
	ROLE	WT	ROLE	WT	ROLE	WT
two-dimensional airfoils						
upper surface inlet flow						
VTOL fan-in-wing						